



Francisco Luís Araújo do Carmo

Graduation in Engineering of Micro and Nanotechnologies

Study on production methods of Bioglass Porous Structures for Bone Tissue Engineering

Dissertation to obtain the Master's Degree in
Engineering of Micro and Nanotechnologies

Advisor: João Paulo Borges, Professor Auxiliar, FCT-UNL

Co-Advisor: Jorge Carvalho Silva, Professor Auxiliar, FCT-UNL

Panel:

Chairperson Hugo Manuel Brito Águas

Rapporteur Célia Maria Reis Henriques

Rapporteur João Paulo Miranda Ribeiro Borges



FACULDADE DE
CIÊNCIAS E TECNOLOGIA
UNIVERSIDADE NOVA DE LISBOA

May, 2018

Study on production methods of Bioglass Porous Structures for Bone Tissue Engineering

Copyright © Francisco Luís Araújo do Carmo, Faculty of Science and Technology, NOVA University of Lisbon

The faculty of Science and Technology and the NOVA University of Lisbon have the right, forever and without geographical limits, to file and publish this dissertation through printed copies reproduced in paper or by digital means, or by any other mean known or that may be invented, and to disclose it through scientific repositories and to allow its copyright and distribution for non-commercial educational or research purposes, provided that the author and editor are credited.

Copyright © - Todos os direitos reservados. Francisco Luís Araújo do Carmo; Faculdade de Ciências e Tecnologia, Universidade Nova de Lisboa.

A Faculdade de Ciências e Tecnologia e a Universidade Nova de Lisboa têm o direito, perpétuo e sem limites geográficos, de arquivar e publicar esta dissertação através de exemplares impressos reproduzidos em papel ou de forma digital, ou por qualquer outro meio conhecido ou que venha a ser inventado, e de a divulgar através de repositórios científicos e de admitir a sua cópia e distribuição com objetivos educacionais ou de investigação, não comerciais, desde que seja dado crédito ao autor e editor

Acknowledgements

First I would like to show my appreciation for the provided help, patience and availability that my advisor Professor João Paulo Borges offered throughout the several months to complete this study.

To my co-advisor Professor Jorge Carvalho Silva I thank all the explanations and suggestions given as well as the work done in the biological stage of this work.

To all the people who worked alongside with me in the “Laboratório de polímeros”: D. Augusta, Dr. João Canejo, Ana Almeida, Catarina and Dr^a. Susete I want to say thank you not only for the help provided but also for the proximity.

To the Professors Maria do Carmo Lança, Maria Margarida Lima and Regina Monteiro, I thank the help and equipment provided for the several tests and processes.

I'm also very thankful for all the good moments and for the support in desperation times given by some colleagues: Diogo Ramos, Andreia Lopes, Luís Martins, André Lopes, Cláudia Gouveia, Diogo Saraiva, Ana Gaspar and António Almeida who accompanied me through most of the work stages, helping me to achieve my goals.

I also would like to mention my college friends and housemates with whom I spend so much time and moments which I will never forget: João Mota, Bernardo Canelas, Mariana Barros, Marcos Rodrigues, Miguel Morais and Alexandre Mogárrio, thank you all for letting me be myself and help me grow as a person.

A special thanks to my big friend and colleague Eduardo Pontes for all things he taught me in the 3D printing area, all the long conversations, meals proportioned, relaxing breaks from the work that he kept pushing me to, for the videogame sessions and above all, for the friendship, that I'm sure will last for long.

A special thanks to the people who made this possible and that believed in me to accomplish the end of this journey. The people who showed their support no matter what, when or where. The people who always received me with open arms after long waiting months without seeing me or even hearing from me. To my family, my deepest of thanks.

And lastly but definitely not the least, to a very special person that I had the pleasure to meet in these long years, without her my life wouldn't have so much colour. Marina, I thank you for all the love that kept me sane.

Resumo

O objetivo deste trabalho consistiu em estudar e produzir estruturas porosas à base de biovidro para aplicação como substituinte ósseo. Três métodos distintos de produção de estruturas foram usados assim como vários tipos de biovidro produzidos por sol-gel, como o 45S5 (45% SiO₂; 24,5% CaO; 24,5%Na₂O; 6% P₂O₅), o 80S20CC (80% SiO₂; 20% CaO) e o 80S5P15C (80% SiO₂; 5% P₂O₅; 15% CaO) (% mol).

Primeiramente estudou-se a fabricação de réplicas invertidas de cristais coloidais (ICCs). Para este efeito produziram-se microesferas de poliestireno por um processo de microfluídica. As esferas (~300 μm) foram depois introduzidas e organizadas numa estrutura hexagonal compacta centrada em poços de uma placa feita de Teflon. De seguida fez-se um tratamento térmico de maneira a que o poliestireno atingisse a transição vítrea permitindo a formação dos Cristais Coloidais (CCs). Utilizando diversos métodos de impregnação do sol-gel de maneira a preencher todo o espaço vazio entre as esferas dos CCs e fazendo tratamentos térmicos a mais de 900 °C para promover a densificação do material, não foi possível criar uma estrutura devido à reduzida massa de biovidro que se conseguiu impregnar nos CCs.

Para o segundo método foi utilizada a técnica de liofilização. Na produção de sol-gel estudaram-se diferentes concentrações de sólidos a 10, 12,5 e 15%. Estas soluções foram introduzidas em seringas, congeladas usando azoto líquido e liofilizadas. Apesar de algumas estruturas terem sido produzidas, estas possuíam muita irregularidade de poros o que as tornou frágeis e difíceis de manusear. Um processo de sinterização foi feito na tentativa de as densificar mas sem sucesso.

Numa outra abordagem, a produção de um cimento à base de biovidro foi feita com a finalidade de obter estruturas porosas por impressão 3D. Dentro dos vários passos de otimização do método de produção, a otimização da pasta a imprimir e dos parâmetros de impressão foram os mais importantes. Após estes melhoramentos estruturas 3D foram impressas e sinterizadas a 1100 °C. Através de imagens de microscopia eletrónica de varrimento (SEM) foi possível verificar a presença de uma superfície porosa. A densidade e porosidade das estruturas foi avaliada e obtiveram-se valores de densidade de 1,43 g/cm³ e de porosidade a 42%. Em estudos de compressão mecânica o máximo valor atingido foi de 6,5 MPa para a resistência à compressão e o módulo de Young foi calculado tendo-se obtido valores na ordem dos 80 MPa. Estudos de DRX e FTIR permitiram identificar a presença de fosfatos de cálcio amorfo e a presença de silicatos em amostras sinterizadas a 1100 °C.

Palavras-chave: Biovidro, ICCs, cimentos à base de biovidro, impressão 3D, engenharia de tecido ósseo.

Abstract

This work's objective was to study and produce bioglass based porous structures for bone tissue engineering. Three different production methods were studied as well as different bioglass sol-gel systems such as: 45S5 Bioglass (45% SiO₂; 24,5% CaO; 24,5%Na₂O; 6% P₂O₅), 80S20CC Bioglass (80% SiO₂; 20% CaO) and 80S5P15C (80% SiO₂; 5% P₂O₅; 15% CaO) (% mol).

In the first method a study on inverted colloidal crystals (ICCs) was made. To achieve these type of structure polystyrene microspheres were produced through a microfluidic apparatus. Microspheres (~300 μm) were then introduced in a Teflon container to organize them into a hexagonal closed pack structure. Posteriorly a thermal treatment was made to promote the adhesion between spheres allowing for the production of the Colloidal crystals (CCs). Using different methods, bioglass sol-gel impregnation was achieved and thermal treatments above 900°C were performed to promote densification. Unfortunately, it was not possible to produce an ICC structure due to the reduced mass of bioglass that was impregnated in the CCs..

For the second method, the technique of lyophilization was used. In the sol-gel production, different solids concentrations were studied at 10, 12.5 and 15%. These solutions were filled into syringes, frozen using liquid nitrogen and lyophilized. Although some structures were produced, they had a lot of pore irregularity which made them brittle and difficult to handle. A sintering process was done in an attempt to densify them but without success.

In another approach, the production of a bioglass based cement was done with the purpose of obtaining 3D printed porous structures. Within the various optimization steps of the production method, the optimization of the printing slurry and the printing parameters were the most important. After these improvements, 3D structures were printed and sintered at 1100 °C. Scanning Electron Microscopy (SEM) images allowed the presence of a porous surface to be detected. The density and porosity of the structures were evaluated. Density values of 1,43 g/cm³ and porosity of 42% were obtained. In mechanical compression studies the maximum value reached was 6.5 MPa for the compressive strength and Young's modulus was calculated with values in the order of 80 MPa. XRD and FTIR studies allowed to identify the presence of amorphous calcium phosphates and the presence of silicates in sintered samples at 1100 °C.

Keywords: Bioglass, ICCs, bioglass based cement, 3D printing, bone tissue engineering

Table of contents

Acknowledgements	v
Resumo	vii
Abstract	ix
1 Objective.....	1
2 Introduction.....	3
2.1 Bioglass	3
2.2 Fabrication of 3D scaffolds.....	4
2.2.1 Inverse colloidal crystals.....	4
2.2.2 Freeze Drying of BGs	5
2.2.3 3D printing	5
2.3 Studies on Bioglass scaffolds.....	6
3 Materials and Methods	9
3.1 Sol-gel synthesis of Bioglasses.....	9
3.2 Microspheres and Colloidal Crystals production	9
3.3 Colloidal crystals impregnation with Bioglass	9
3.4 Freeze-drying of BG	10
3.5 3D printing of Bioglass cement.....	10
3.6 Characterization	10
3.6.1 Optical microscopy	10
3.6.2 Scanning Electron Microscopy (SEM).....	10
3.6.3 Fourier-transform infrared spectroscopy (FTIR).....	11
3.6.4 Mechanical	11
3.6.5 Cytotoxicity and cell viability.....	11
3.6.6 DSC-TG.....	11
3.6.7 X-Ray Diffraction	11
3.6.8 Densification study	11
3.7 Flowchart of 3D structures production.....	11
4 Results and Discussion	13
4.1 Microspheres and CCs	13

4.1.1	Microspheres diameter and roundness	13
4.1.2	Optical Microscopy of CCs	14
4.2	Density studies of 45S5 Bioglass	14
4.3	Impregnation of CCs with bioglass	15
4.4	Freeze-drying of bioglass sol-gel	17
4.5	3D printing of bioglass cement	18
4.5.1	Optimization process	18
4.5.1.1	Slurry	18
4.5.1.2	Printing parameters	20
4.5.2	Optical microscopy and Scanning Electron Microscopy (SEM)	20
4.5.3	DSC-TG	21
4.5.4	X-Ray Diffraction	22
4.5.5	FTIR.....	23
4.5.6	Mechanical characterization.....	24
4.5.6.1	Compressive strength and elastic modulus	24
4.5.6.2	Porosity study (Archimedes method)	24
4.5.7	Cytotoxicity	26
5	Conclusion and Future perspectives	29
6	Bibliography.....	31
	Appendix I	35
	Appendix II	37
	Appendix III	39
	Appendix IV	41
	Appendix V	42

List of Figures

Figure 2.1 – The three main steps to produce an inverse colloidal crystal. A – Polystyrene microspheres. B – Colloidal crystal. C – Representation of the wanted ICC [4].	4
Figure 2.2 – Picture of a structure being printed in the current work.	5
Figure 3.1 – Schematic representation of the microspheres production method and an illustration of the CC template. Adapted from Choi et al. [25].	9
Figure 4.1 – Optical microscope image of polystyrene microspheres obtained with the selected production parameters.	13
Figure 4.2 – Optical microscopy images of one CC structure and some defects.	14
Figure 4.3 – Graph of the density studies on 45S5 Bioglass pellets sintered at 900, 1000 and 1100 °C.	15
Figure 4.4 – Impregnated CCs through centrifugation of Bioglass sol-gel before (A) and after (B) sintering at 1000 °C.	16
Figure 4.5 – Before (C) and after (D) sintering of the freeze dried samples.	17
Figure 4.6 – Simulation of a 3D printer extruder to study the behaviour of the different slurries (E). Resulting structures from the simulation tests (F).	18
Figure 4.7 – Optical microscope image of the wall of a sintered 3D printed structure.	20
Figure 4.8 – SEM image of the side view (G) of sintered structures.	20
Figure 4.9 – SEM images of the top surface of structures sintered at 1100 °C.	21
Figure 4.10 – DSC-TG graphic analysis of the mesoporous 80S5P15C bioglass powder after 600 °C treatment for 2 hours.	21
Figure 4.11 – DSC-TG graphic analysis of the mesoporous 80S5P15C bioglass cement after 24h drying process at 60 °C.	22
Figure 4.12 – Diffractogram of the final cement composition 1100 °C.	22
Figure 4.13 – FTIR spectrum of the mesoporous 80S5P15C bioglass (600 °C).	23
Figure 4.14 – FTIR spectrum of the bioglass cement treated at 1100 °C.	23
Figure 4.15 – Compression curve of a bioglass cement sample after 1100 °C sintering process.	24
Figure 4.16 – Top view of an example structure used in the porosity evaluation with measures and calculations of the real volume.	25
Figure 4.17 – Studies on the porosity and compressive strength of bioactive glass scaffolds. Adapted from [18].	26
Figure 4.18 – Degradation tests in Water (I) and a NaCl solution (J) after 2 weeks.	27

Figure 4.19 – Extract with pH indicator (Phenol red) after neutralization attempt. Yellow colour indicating an acid solution. 27

Figure 20 - Hyrel 30M 3D printer..... 41

List of Tables

Table 2.1 – Principal advantages and disadvantages of some 3D porous structures production methods.....	6
Table 2.2 – Brief description of some studies made in the area of 3D porous structures based on bioglass, contemplating in vitro and in vivo resultsl.	7
Table 4.1 – Results on the study of microspheres diameters.	13
Table 4.2 –Measurements on the impregnated bioglass into CCs by applying centrifugation force.....	15
Table 4.3 – Average % of mass increment in centrifugations with Bioglass containing 1, 3 and 5% PVA.	16
Table 4.4 – Useful printing time study on the slurries combinations.	19
Table 4.5 – Study on the densification and porosity of the material.....	25

List of Symbols and Abbreviations

Abbreviation	Designation
CC	Colloidal crystal
ICC	Inverted Colloidal crystal
Hcp	Hexagonal closed pack
ISISA	Ice-segregation-induced self-assembly
SLS	Selective laser sintering
BG	Bioglass
PVA	Polyvinyl Alcohol
SEM	Scanning Electron Microscopy
FTIR	Fourier Transform Infrared Spectroscopy
XDR	X-ray diffraction
DSC	Differential Scanning Calorimetry
TG	Thermogravimetry
PS	Polystyrene

1 Objective

The aim of this project was the evaluation of different manufacturing techniques to produce 3D microporous/macroporous biocompatible structures for application in bone tissue engineering.

2 Introduction

2.1 Bioglass

Bone tissue engineering has gathered a lot of attention amongst the scientific community in the past several decades. In the late 1960s, a breakthrough discovery led to very relevant results respecting to bone tissue regeneration *in vivo*. It was in that time that Larry L. Hench “gave birth” to the 45S5 Bioglass, and published his first paper on the subject in 1971.

45S5 Bioglass is a bioactive material which has in its composition a 45% of SiO₂, 24.5% CaO, 24.5% Na₂O and a 6% P₂O₅, making a 5:1 ratio of Ca/P, all in wt%. SiO₂ provides a slow degradation rate of the present ions and gives the glass the amorphous structure, and thus, stability. The Ca/P ratio pretends to establish a balance between the material and the ratio present in Hydroxyapatite found in bones. Na⁺ ions are easily dissolved, and help with the interactions between the material/medium interface, by equalizing the sodium content and pH conditions [1]. This composition allows a great osteoconductivity and osteoinductivity, making this material a class A, in terms of bioactivity. After production and further treatment, when in contact with physiological medium, the release of Ca²⁺, PO₄³⁻ and Na⁺ ions forms an apatite layer which will then promote the bonding with living tissue [2], [3].

For a bone substitution intervention to be successful, the substitute material has to follow some minimum requirements, especially regarding its similarity with the bone's physical structure, cortical or cancellous, and chemical composition, to allow connection between tissue and material. Aiming to the physical structure of a substitute material, the rule to follow is “the stronger the better”, as these substitutes may need to support temporarily all the stress that a normal bone would have to experience. But, like bone itself, the structure must also be very porous to allow osteoblasts to migrate, proliferate and replicate, which might compromise the mechanical properties required. The size of the connections between porous must be greater than 50 μm since osteoblasts have an average diameter of 20 – 30 μm. As to chemical composition, biocompatibility and biodegradability are a must, and to achieve this goal the material should be made out of similar phases that are found in bone. Biocompatibility/bioactivity prevents the fibrotic reaction and further rejection of the substitute and promotes the bone reconstitution process, as for the biodegradability, it allows the natural removal of the structure while being replaced with bone tissue [4].

After the discovery of the 45S5 Bioglass, other studies started to make slight changes in its composition, while others made more deep alterations creating a wide variety of Bioceramics. These bioglasses can have great variations in percentage of components, yet, the main ones are Silicon or Borate (40 to 85%), Calcium (10 to 30%), Phosphorous (0 to 10%) and Sodium (0 to 30%). Other elements like Aluminium, Copper, Zinc and Strontium can be part of the glass but only in low percentages. (Aluminium – 0 to 1.5%) [5], [6].

2.2 Fabrication of 3D scaffolds

To produce a scaffold that meets all the required characteristics to become a substituent material for bone tissue engineering, a variety of methods can be found in literature. A great number of studies made in this field of expertise involve techniques such as porogen leaching, phase separation, gas foaming, emulsion freeze drying, electrospinning, 3D printing, extrusion, selective laser sintering, solid free-form fabrication, and rapid prototyping, all with their strengths and weaknesses [4]. In this work the following three approaches were used: inverted colloidal crystal scaffolds, freeze drying and 3D printing.

2.2.1 Inverse colloidal crystals

These structures can have a minimum porosity of 74% and a 100% pore interconnectivity. They are produced by replication of a 3D construct made by packing of monodisperse spheres as template, the colloidal crystal (CC). The connection of the spheres can be made by thermal treatment or by using a “glue material” usually a polymer. Once the CC is made, the material of interest can be inserted between spheres and left to dry, after drying the spheres are removed by a degrading agent, or by spheres leaching with thermal treatment, leaving as a remain a porous structure, known as Inverted Colloidal Crystal (ICC). The fabrication of a reliable ICC lies on a good size monodispersivity of the microspheres used and in the good settling and hexagonal-closed-pack (hcp) organization of the same spheres to provide the ideal 100% interconnectivity between pores. Any defects in spheres or organization can lead to a decrease in interconnectivity and mechanical resistance as these flaws will propagate through the structure leading to disordered parcels.

The characteristics of ICCs such as pore size and pore connection width can be tuned. Pore size is mainly affected by spheres size. The width of interconnections between pores can be modified by changing the temperature or time of thermal treatment. In the case where a “glue material” is used changing the concentration of that solution will affect the width, since the viscosity plays an important role [4], [7], [8], [9].

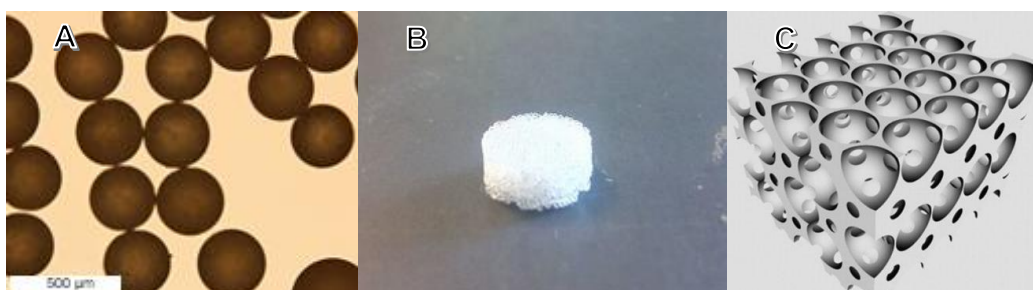


Figure 2.1 – The three main steps to produce an inverse colloidal crystal. **A** – Polystyrene microspheres. **B** – Colloidal crystal. **C** – Representation of the wanted ICC [4].

2.2.2 Freeze Drying of BGs

Complex structures that have sophisticated patterns are many times based on processes that occur in nature. In most of these processes water is the only solvent readily available. Given this, nature itself has perfect and optimized the processing of functional materials using water. The design and use of aqueous processes capable of maintaining an already existent structure and introducing further levels of spatial organization to the same would be a great step towards the preparation of highly complex and hierarchically organized structures [10].

The formation of crystalline ice (hexagonal ice) is the source of the self-assembly and organization of structures made by this technique. The orientation of the aqueous solution makes every existent solute to be forced out of the ice crystals becoming trapped in between them [10]. Then, with the assist of high-vacuum sublimation of ice, all that's left behind are the solutes organized in a macro porous network. In the last decade, the ice-segregation-induced self-assembly (ISISA) process has gathered considerable attention due to its development in macropore orientation in scaffolding. The combination of this process with unidirectional freezing using liquid nitrogen, makes it possible to control the growth direction of ice crystals, as well as the template [11].

2.2.3 3D printing

The 3D printing technique provides great advantage in terms of shape control. The base material used is a filament or a paste and, as a form of rapid prototyping, it provides an easy and quick way to obtain 3D structures in a layer-by-layer deposition using a computer-aided design. A well-defined structure can be easily achieved after the optimization processes of the extruded material and printing parameters.

The quality of 3D printing will always depend on the equipment used, but it has been proven that prints of anatomical structures with great detail could be produced, when compared to the original specimens [12]. The 3D printing has proportioned many new paths for the rapid production of objects in a great variety of fields. Particularly in the anatomical field, it has allowed for a more detailed production of structures and according to Y. AbouHashem *et al.* "It appears to be particularly easy to implement in producing bone models" [13]. It's very likely that in the next coming years the number of applications of this technique will rise as the equipment cost starts to drop [14].

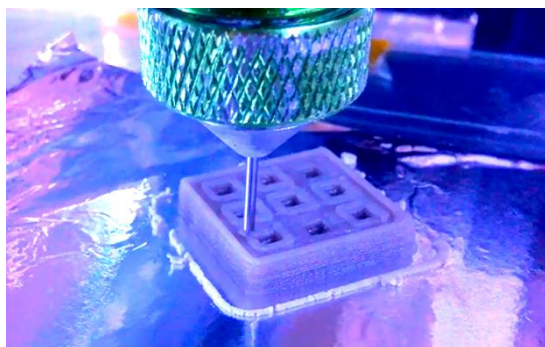


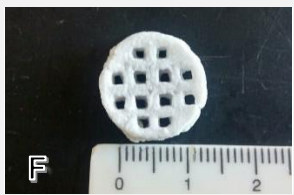
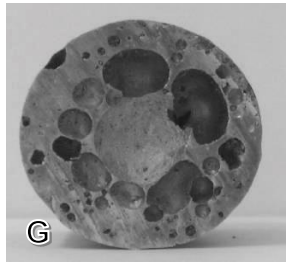
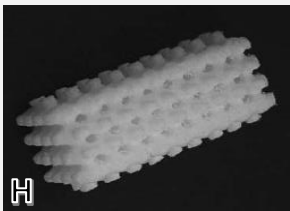


Figure 2.2 – Picture of a structure being printed in the current work.

Table 2.1 – Principal advantages and disadvantages of some 3D porous structures production methods. **D** - [8], **E** - [15], **F** - Current work, **G** - [16], **H** - [17].

Method	Advantages	Disadvantages	Examples
Inverted Colloidal Crystals (ICCs)	<ul style="list-style-type: none"> ➤ Excellent organization; ➤ Interconnectivity; ➤ Uniformity; ➤ Cheap. 	<ul style="list-style-type: none"> ➤ Mechanical strength; ➤ Hard to impregnate with wanted material; ➤ Very difficult to process at large scale. 	
Freeze drying (ISISA assisted)	<ul style="list-style-type: none"> ➤ Sub micrometric porosity; ➤ Good organization. 	<ul style="list-style-type: none"> ➤ Specific equipment required; ➤ Slow process; ➤ Mechanical strength. 	
Solid freeform fabrication (3D printing)	<ul style="list-style-type: none"> ➤ Quick, easy and cheap; ➤ Design freedom; ➤ Easy to scale. 	<ul style="list-style-type: none"> ➤ Pore size limitations; ➤ Requires extensive optimization; 	
Gas foaming	<ul style="list-style-type: none"> ➤ Solvent-free. 	<ul style="list-style-type: none"> ➤ Random pores; ➤ Interconnectivity; ➤ May need further processing. 	
Selective Laser Sintering (SLS)	<ul style="list-style-type: none"> ➤ Precision; ➤ Offers support to make hang structures in a sample (bridges). 	<ul style="list-style-type: none"> ➤ Only works in some powders; ➤ Specific equipment required. 	

2.3 Studies on Bioglass scaffolds

Bioglass scaffolds have been studied for decades, and some compositions of bioglass have been available in the market for more than 20 years. Comprehensive study regarding the production and mechanical properties of porous bioactive glass scaffolds can be found in the review of Q. Fu et al. [18]

Examples of *in vitro* and *in vivo* studies involving scaffolds of various bioglass based materials, are listed in the table 2.2, alongside with the production method of the template and a summary of the results obtained.

Table 2.2 – Brief description of some studies made in the area of 3D porous structures based on bioglass, contemplating *in vitro* and *in vivo* results.

Type of bioglass or composite	Scaffold fabrication and treatment	Scaffold characteristics	<i>In vivo</i> species used and/or <i>in vitro</i> studies	Results
45S5 Bioglass (Melt-Derived) [19]	Dry pressing and sintering with 20,2% camphor particles. 630°C for 30 minutes.	Macroporosity – 21% Pore size between 200 and 300 µm Crystallinity – 40%	Species – Femoral diaphysis of Fisher 344 rats Primary - <i>In vitro</i> treatment with bone marrow stromal cells to promote production of a mineralized extracellular matrix. Cells were placed on top of the scaffolds and left for 2 hours to attach. Hybrid – Same treatment as Primary, but the scaffold was immersed in the cell culture medium for 2 weeks.	Primary - direct evidence of bone formation from the scaffold could not be detected by bone labelling. Hybrid - At 2 weeks implantation, for the hybrid, woven bone grew from the scaffold out towards the cortical edge and within the outer surface macropores and microcracks.
Mesoporous Bioactive Glass (Sol-Gel Derived) [20]	Infiltration of the solution into Polyurethane foams and sintering at 700°C for 6h. Immersed in SBF for 10 days	Pore size between 300 and 500 µm	Species - Bilateral femoral condyles of Sprague–Dawley rats	<i>In vivo</i> - The histological analysis showed that the MBG scaffolds were adsorbed and that new bone invaded the scaffolds, from the edge to the centre, from weeks 4 to 12 post implantation.
13-93 Bioglass (Melt-Derived) [21]	Unidirectional freezing with camphene based suspensions, followed by sublimation of camphene particles and further sintering at 700°C for 1h.	Porosity - 50±4% Pore size between 50 and 150 µm Compressive strength - 47±5 MPa	Species – Calvaria of Sprague–Dawley rats Treatment - 10% buffered formaldehyde for 3 days, transferred to 70% ethyl alcohol. After dehydration and cutting process they were embedded in PMMA.	Total bone regeneration - 37±8% and 55±5% at 12 and 24 weeks, respectively. (% of area available) Total mineralized area – 58±5% and 68±5% for 12 and 24 weeks, respectively.
Phytic acid-derived bioglass (PSC/CS) cement [22]	No scaffold, just a solid injected cylinder.	Compressive strength - 2.9 MPa Young's modulus - 340 MPa	The <i>in vitro</i> test showed that the cement was bioactive, biocompatible and could maintain its shape sustainably, which made it possible to provide a long-term mechanical support for bone regeneration.	At 4 weeks no significant change was observed. At the 8th week, resorption of the cement was noticeable. At the 12th week, new bone was formed at the cement-bone interface.
70S30C Bioglass (Sol-Gel Derived) [23]	Foaming technique [24]. Sintering at 800°C for 2h.	Macroporosity – under 90% Interconnectivity – 54% of interconnects ≥ 100 µm Pore size – 100 to 400 µm	Species – Medial aspect of the tibia of Wistar rats Immersion on serum free α-MEM medium, for 5 minutes or 3 days.	61% of the material made contact with new bone. After 11 weeks <i>in vivo</i> , histological analysis of samples revealed thick cortical bone around the residual 70S30C material.

3 Materials and Methods

3.1 Sol-gel synthesis of Bioglasses

In this work, 3 main Bioglasses were produced with the following compositions:

- 45S5 Bioglass: 45% SiO₂, 24,5% CaO, 24,5% Na₂O, 6% P₂O₅ (Wt%)
- 80S20C Bioglass: 80% SiO₂, 20% CaO (mol%)
- 80S5P15C Bioglass: 80% SiO₂, 5% P₂O₅, 15% CaO (mol%)

The precursors used were:

- Silicon - Tetraethyl orthosilicate (Si(OC₂H₅)₄);
- Phosphorous - Triethyl Phosphate ((PO(C₂H₅)₃);
- Calcium - Calcium Nitrate tetrahydrate (Ca(NO₃)₂·4H₂O);
- Sodium - Sodium Nitrate (NaNO₃).

For details in the production methods view Appendix I.

3.2 Microspheres and Colloidal Crystals production

A schematic representation of the production method is presented in the figure 3.1. This method was based on the work of Choi *et al.* [25], and detailed information of the procedure is presented in the Appendix II.

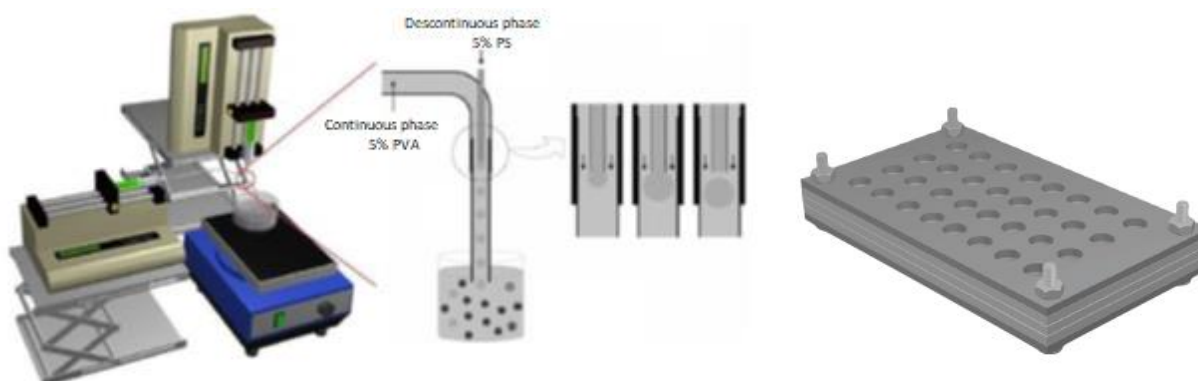


Figure 3.1 – Schematic representation of the microspheres production method and an illustration of the CC template. Adapted from Choi *et al.* [25].

3.3 Colloidal crystals impregnation with Bioglass

Polystyrene CCs were impregnated through several different approaches: manual impregnation of the BG, manual impregnation with 0,25, 0,75 and 1,25% PVA mixed with BG, CC into the BG gel under vacuum, centrifuge cycles, impregnation mid BG synthesis under vacuum, forcing the sol-gel into the CC using a syringe (positive pressure) or using combinations of these methods. After drying, all impregnated CCs were sintered or immersed in dichloromethane to melt

or dissolve the polystyrene template. The detailed aspects on the procedures are presented in Appendix III.

3.4 Freeze-drying of BG

To obtain porous structures through freeze-drying, several attempts were performed with different types of BGs and different solid content (%) in the sol-gel solution. The tested BGs were: i) 45S5 Bioglass; ii) 45S5 Bioglass but with half Sodium percentage; III) Sodium free 45S5 Bioglass; iv) the 80S20C Bioglass and v) the 80S5P15C Bioglass. All of these were tested for solid content percentages of 10, 12,5 and 15%. After the production of bioglass and further dilutions, they were introduced in a syringe and left to freeze in a – 10 °C freezer. After several hours the syringes were merged in liquid nitrogen for 10 minutes and posteriorly introduced in the freeze dryer (VaCo 2, Zirbus) for 2 to 3 days. Some samples were then sintered to evaluate densification.

3.5 3D printing of Bioglass cement

This method was performed using only the 80S5P15C Bioglass, made with and without Pluronic F-127. A study and optimization of the slurry composition was made and several components were tested: Glycerine, Tween 20, Oleic Acid, PVA and a buffer solution made with Alginic Acid Sodium Salt, Ammonium di-Hydrogen Phosphate and Ammonium Phosphate dibasic. The objective here was to create a slurry capable of maintaining stability for at least 30 minutes in order to be printed. Final composition: 35% bioglass powder, 16% Tween 20 and 49% buffer solution with 2.5% Alginate. After mixing, the slurry was introduced in a syringe and smoothly centrifuged to take out all the air bubbles, inserted in the 3D printer support and printed at room temperature and ambient conditions. Information on the reagents and equipment in Appendix IV.

3.6 Characterization

3.6.1 Optical microscopy

Through optical microscopy several samples of microspheres were measured and their shape was evaluated. All measurements were performed with ImageJ software on, at least, 100 samples at a time.

Colloidal crystals were also examined with respect to structure and to assess their viability.

3D printed structures were also examined for porosity and surface roughness.

3.6.2 Scanning Electron Microscopy (SEM)

SEM images were taken with a Hitachi Tabletop Microscope TM3030 series.

3.6.3 Fourier-transform infrared spectroscopy (FTIR)

FTIR spectrums were obtained with a Spectrum Two FT-IR Spectrometer from PerkinElmer.

3.6.4 Mechanical

Compressive strength characterization was only performed in samples produced by 3D printing in the final format. Uniaxial mechanical force was applied by a Universal Electromechanical Test Frame (Shimadzu) with a 50 kN load cell until fracture occurred, at a speed of 0,5 mm/min. Samples mean area was 260 mm².

3.6.5 Cytotoxicity and cell viability

As an attempt to determine the material's cytotoxicity and cell viability the extract and resazurin methods were used. All the steps and details of the method are described in the Appendix V.

3.6.6 DSC-TG

Thermal gravimetry and differential scanning calorimetry analysis were performed in different types of bioglass in order to evaluate the better parameters for the sintering steps. Materials were heated at a 10 °C/min rate until 1200 °C.

3.6.7 X-Ray Diffraction

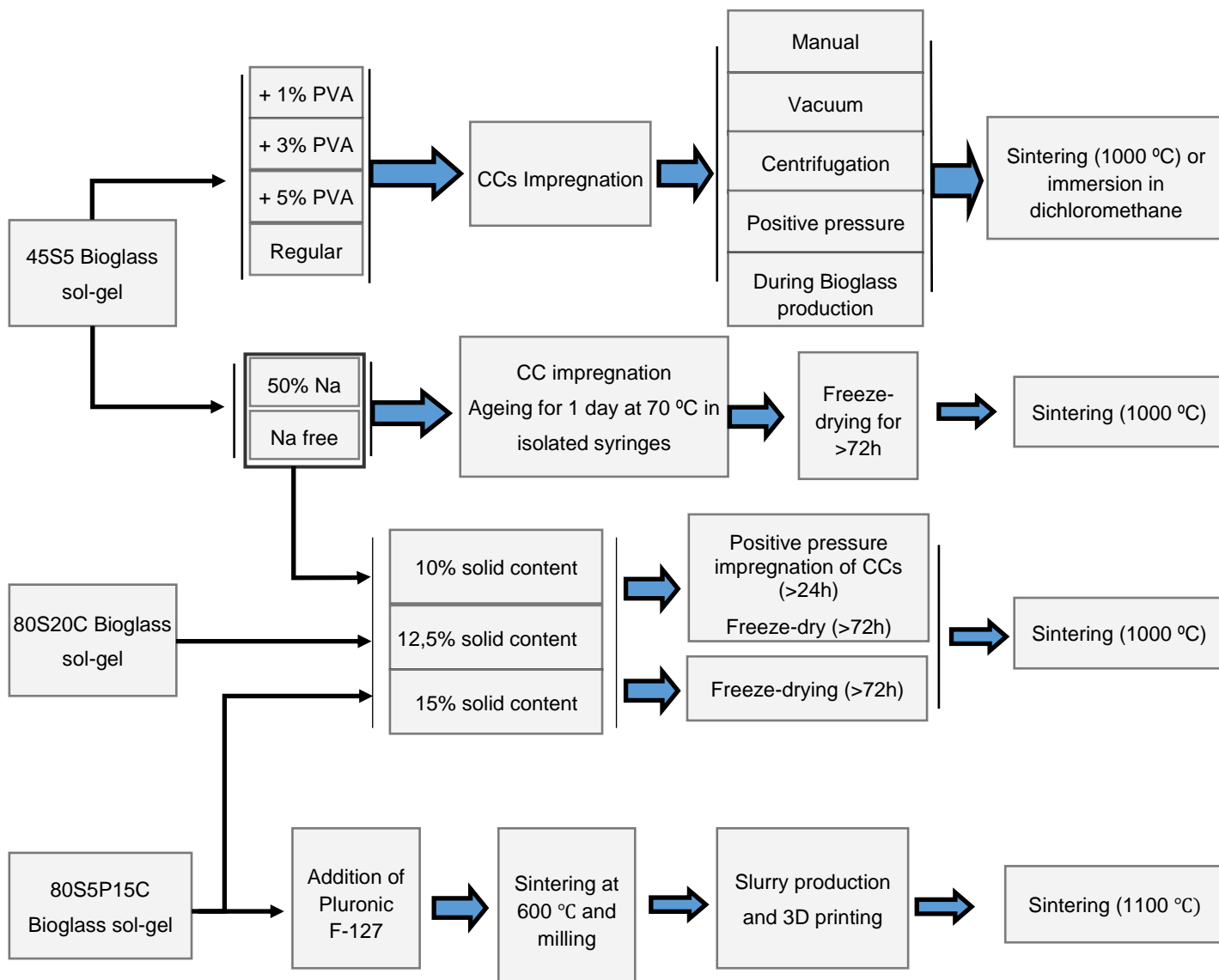
Wide angle X-ray diffraction was performed to identify the crystalline phases of the final samples made of 80S5P15C Bioglass cement after sintering. The measurement equipment, a X^{pert} PRO (PANalytical) X-ray diffractometer, using CuK α radiation generated at 45 kV and 40 mA, scanned the sample in the range $0^{\circ} \leq 2\theta \leq 90^{\circ}$. Peaks were compared and identified through Match! Software.

3.6.8 Densification study

In another characterization of the 80S5P15C Bioglass cement a densification test was made using the same heating parameters as the sintering process to evaluate if, and at what temperature, densification occurs. Porosity was evaluated by the Archimedes method on cylindrical tablets sintered at 900, 1000 and 1100 °C.

3.7 Flowchart of 3D structures production

For a better understanding of the several steps followed in the production of porous structures, a flowchart is presented.



4 Results and Discussion

4.1 Microspheres and CCs

4.1.1 Microspheres diameter and roundness

Considering previous works that used the same method to produce polystyrene microspheres, information was gathered with respect to flow values of the continuous and discontinuous phases. As the capillary tube used in the most recent production had a higher diameter than the previous one, new test values were considered for both flows and needle diameters. With the objective of obtaining spheres between 250 and 400 μm , the following table shows the results of the different experiments. For these tests, a 0,7 mm diameter needle was used for the continuous phase and a 0,5 mm for the discontinuous phase.

Table 4.1 – Results on the study of microspheres diameters.

Continuous phase flow (PVA 5%) in mL/h	10	10	10	9	9	20
Discontinuous phase flow (PS 5%) in mL/h	4	5	6	5	6	3
Mean diameter in μm	296 \pm 41	261 \pm 34	234 \pm 27	300 \pm 9	300 \pm 18	262 \pm 38

The shown results only represent the experiments in which good roundness of the beads was obtained. After analysing the results, all of the production of microspheres was made with 9 mL/h continuous phase and 5 mL/h discontinuous phase.

Microspheres' morphology was observed and evaluated through optical microscopy to ensure good organization in the CCs production.

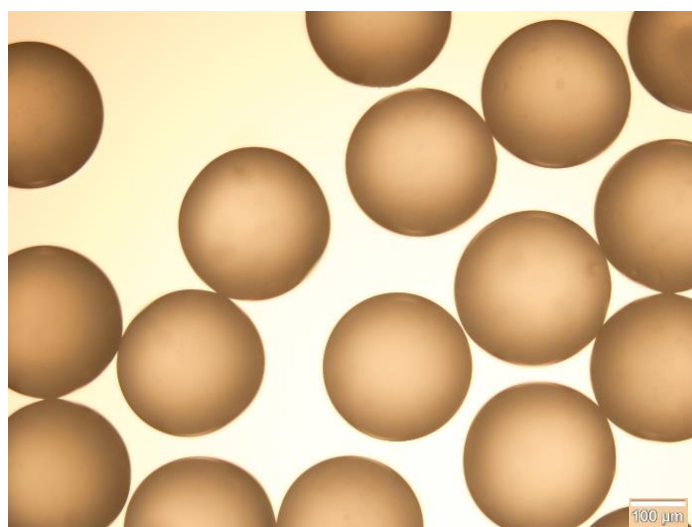


Figure 4.1 – Optical microscope image of polystyrene microspheres obtained with the selected production parameters.

Sieving of the spheres with 4 different mesh sizes (212, 250, 280 and 300 μm) was performed and once again they were observed and measured to assure the sieving objective was obtained.

As observed in the figure 4.1, good sphericity was achieved. The measurements analysis after the sieving process showed that the several meshes were in good state.

4.1.2 Optical Microscopy of CCs

CCs organization and structure was observed through optical microscopy to evaluate their viability. Figure 4.2 shows some images of good organization and also some defects.

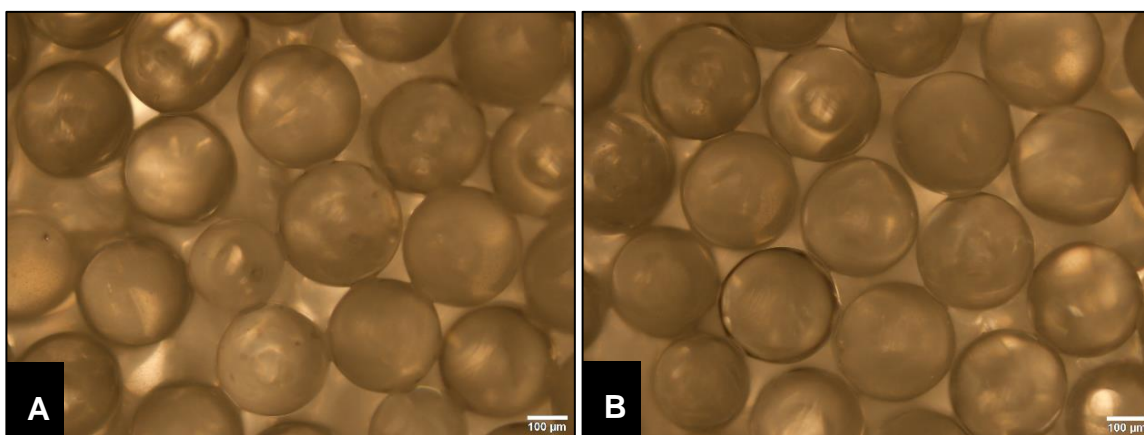


Figure 4.2 – Optical microscopy images of one CC structure and some defects.

After the annealing process, some defects were encountered when analysing the CC's microphotographs. As spheres have a relatively large gap of sizes even after sieving ($>50 \mu\text{m}$ in the 300 to 355 μm interval) and not every one of them are perfect spheres, defects as lack of interconnections or irregular links were expected, as shown in image A. In B, a good organization was visible in this portion of the CC but still, some defects are evident. All produced CCs presented these types of defects, as the microspheres production process still lacks some improvement, as well as the accommodation of the spheres in a hexagonal close pack to form the CC's template.

4.2 Density studies of 45S5 Bioglass

A brief study on the densification of the 45S5 bioglass revealed that the peak density of the material is achieved at near 1000 $^{\circ}\text{C}$. Moreover, it was observed that at 1050 $^{\circ}\text{C}$ the material started to melt.

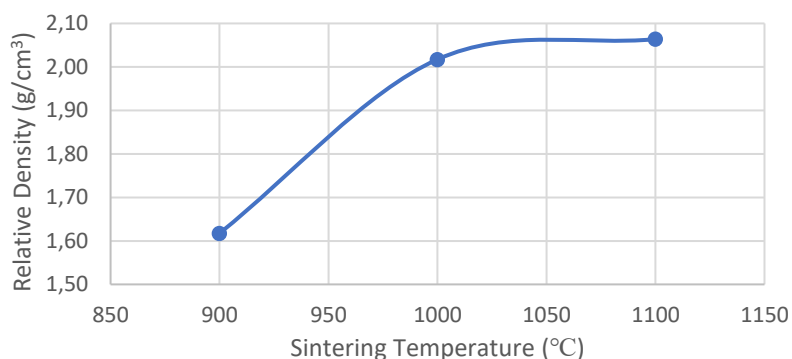


Figure 4.3 – Graph of the density studies on 45S5 Bioglass pellets sintered at 900, 1000 and 1100 °C.

4.3 Impregnation of CCs with bioglass

A key factor to accomplish a good impregnation is the low viscosity of the sol-gel solution. After the bioglass production, a PVA solution was mixed with bioglass with two purposes: a) lower the viscosity and b) help maintain the bioglass slurry stability during the polystyrene CC dissolution.

During this work it was observed that bioglass produced by sol-gel method suffers a great loss of mass and volume after the impregnation of CCs. Given this, many of the impregnation methods used didn't make great progress in the production of ICCs.

The best attempt in which the most quantity of bioglass made its way into the CC structure was the centrifugation method. The maximum value was reached at 5 centrifugations with a mean value of 4,5 mg of CC's weight increment. Further centrifugation cycles showed no significant progress in the mass addition into the CCs. All the CCs used had the same interval of spheres size, 280 to 300 µm, and their weight was measured prior centrifugations.

Table 4.2 –Measurements on the impregnated bioglass into CCs by applying centrifugation force.

Initial weight (mg) / Weight at X cycles (mg)	41,2	41,2	50,8	36,7	47,9	49,2	43,8	44	46,9	38,5	43,2	47,4	49,7	42,1	40,4
X = 1	43,3	42,8	52,7	37,5	49,0	50,9	44,3	45,1	49,3	39,8	44,4	48,7	50,8	43,8	41,9
X = 3	44,1	43,4	55,4	39,0	50,2	52,5	45,8	46,5	51,5	41,2	45,7	49,5	53,1	43,2	43,5
X = 5	44,2	44,1	56,9	40,1	50,8	53,2	45,7	47,7	52,6	41,8	45,9	49,4	54,6	44,9	44,2
X = 7	45,0	43,6	58,0	40,3	50,1	53,7	46,5	48,1	52,5	41,4	45,6	50,2	54,0	45,1	44,9
X = 9	45,1	44,0	57,8	39,9	49,3	53,9	46,3	48,8	52,5	40,1	45,8	51,0	54,6	45,8	44,3
$\frac{\text{Bioglass (mg)}}{\text{CC (mg)}} * 100 (\%)$	9,4	6,8	13,8	8,7	2,9	9,6	5,7	10,9	11,9	4,2	6,0	7,6	9,9	8,8	9,7

1% PVA
 3% PVA
 5% PVA

It is important to refer that some CCs ended up losing some of the constituent spheres during the force application and excess bioglass removal with a smooth brush. This led to a small but considerable error in the measurement of bioglass mass increment. The variation on the PVA

content of the bioglass didn't seem to affect the impregnation process in terms of quantity of material introduced. But with 5% PVA the increment of mass seemed to be slower to achieve the final quantity.

Table 4.3 – Average % of mass increment in centrifugations with Bioglass containing 1, 3 and 5% PVA.

Centrifugations	PVA 1%	PVA 3%	PVA 5%
1	3,4%	3,1%	3,1%
3	6,5%	6,8%	5,5%
5	8,3%	8,3%	7,3%
7	8,7%	8,8%	7,7%
9	8,3%	8,5%	8,4%

It was noticeable that after 5 centrifugations the mass increment lowered considerably and that further cycles didn't result in further progress. The maximum bioglass weight that was able to be impregnated by this method was estimated in 9% of the CCs mass. Sintering process was then performed at 1000 °C and in Figure 4.3 the final result is shown.

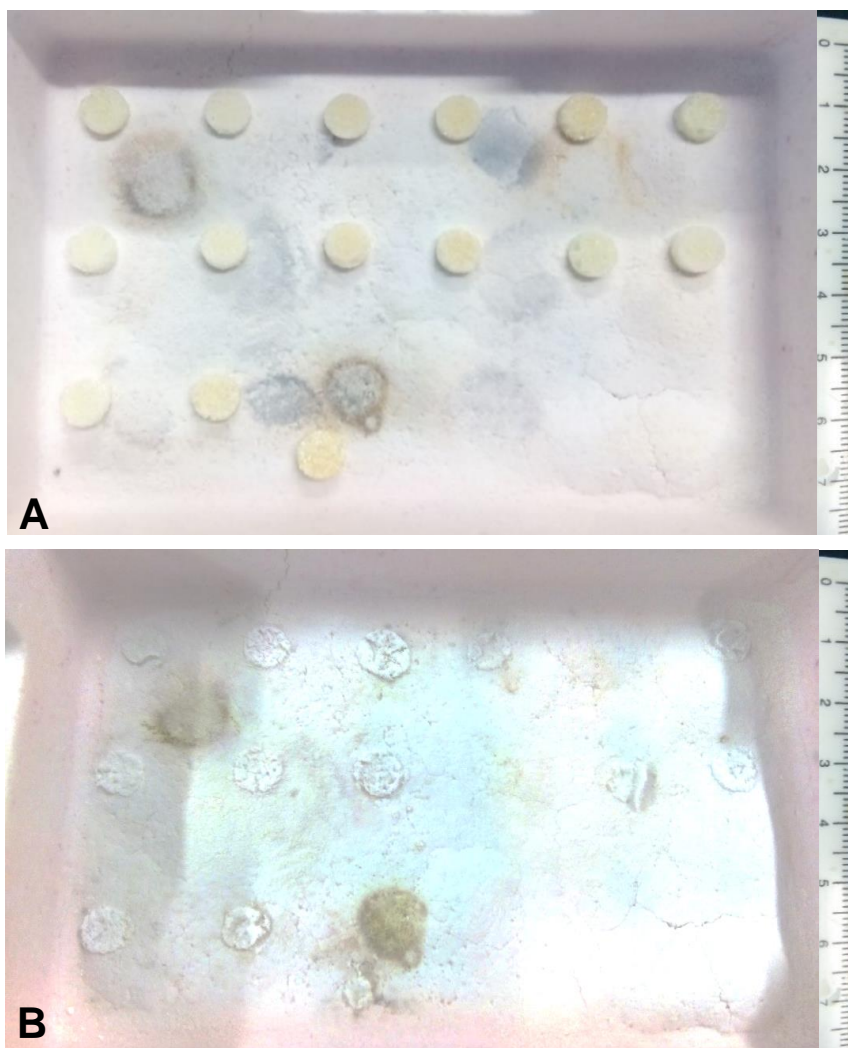


Figure 4.4 – Impregnated CCs through centrifugation of Bioglass sol-gel before (A) and after (B) sintering at 1000 °C.

It was noticeable that bioglass was present inside the CCs, but as the polystyrene starts to melt (90 ~ 240 °C) the bioglass particles started to fall apart due to lack of support.

4.4 Freeze-drying of bioglass sol-gel

In the literature, some studies report the use of the freeze-drying method in bioglass sol-gel systems to obtain a crystalline porous structure. The crystallinity results from the fact that the ISISA process is used in these samples to slowly freeze them unidirectionally and so the ice crystals have an organized assembly. In the current work it wasn't possible for the use of this method, so by only freeze drying the bioglass sol-gel, it was expected that a porous structure would form but with no crystallinity or any particular organization. A combination of freeze drying the bioglass impregnated into CCs was also tested but with very poor results. In the other attempts with many variants of bioglass composition, some structures were produced with relative success. As unidirectional freezing wasn't applied, these structures were much disorganized and large pores were present making the handling of the samples very difficult without collapse. As these fragile structures didn't exhibit any mechanical resistance a sintering process was performed to promote densification of the material.



Figure 4.5 – Before (C) and after (D) sintering of the freeze dried samples.

Even though a porous structure was fabricated through freeze-drying, the loss of mass and volume suffered by the bioglass didn't allow for structure to be maintained. The melting point of

these bioglasses occurred at temperatures above 1050 °C as observed in previous sintering processes.

Given this, and considering the results shown in Figure 4.5, it was hypothesized that a support structure would be needed to maintain the integrity of the porous bioglass during the sintering and densification process. As the support needed couldn't be fabricated, freeze dry method was discontinued as well as CC impregnation.

4.5 3D printing of bioglass cement

4.5.1 Optimization process

4.5.1.1 Slurry

In the optimization process of the slurry, several factors had to be taken into account: powder particles size, powder dissolution, viscosity of the paste, diameter of the nozzle, ease of extrusion of each combination, homogeneity, time of solidification and stiffness of the dried structure.

As the 3D equipment wasn't always available, experiments for optimizing the slurry were carried on with a simulation of the extruder. Inserting the slurry in a syringe and using a Kd scientific injector to act as an extruder, the “useful printing time” (time window in which a slurry can be extruded before it hardens) was obtained with a needle of 0,7 mm diameter.

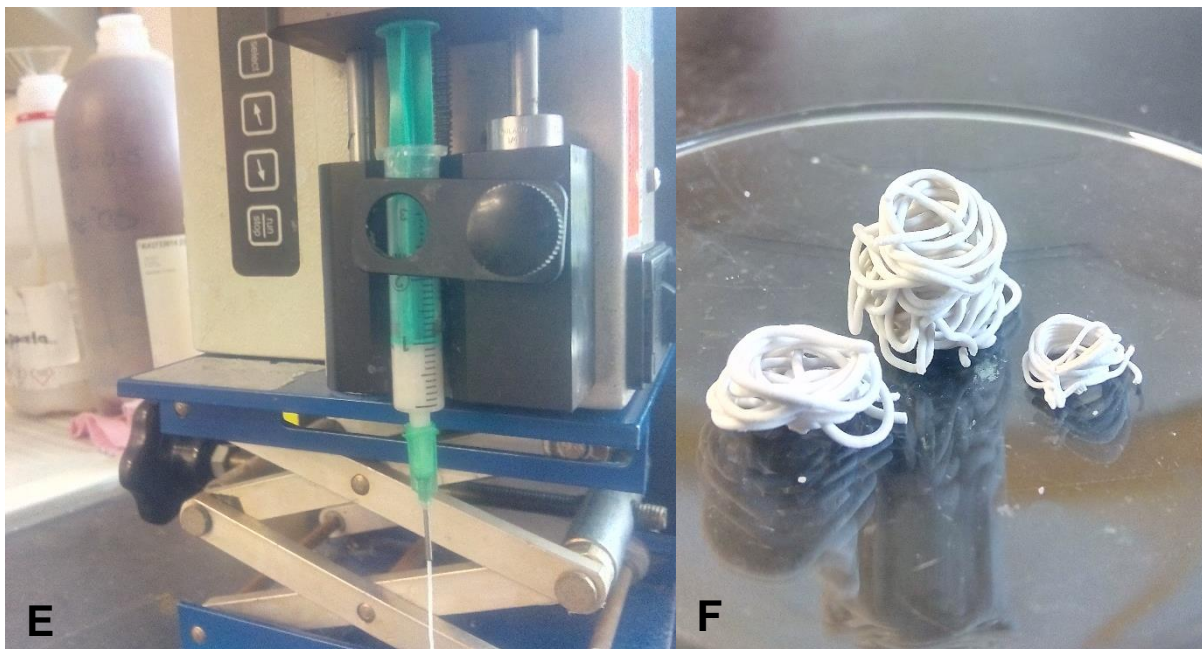


Figure 4.6 – Simulation of a 3D printer extruder to study the behaviour of the different slurries (E). Resulting structures from the simulation tests (F).

The main mixture incorporated the bioglass powder with the phosphate buffer solution as this combination was the key to the solidification of the cement. Several ratios between only these

two components were experimented but the setting time didn't went above the 10 minutes. Other components (plastificants) were then added to provide a smother extrusion such as Glycerine, Oleic Acid, Tween 20 and PVA 5%. The use of glycerine was discontinued due to the lack of homogenization of the slurries. It was noticed that slurries containing Glycerine wouldn't stay stable after applying pressure with the piston. The same problem occurred when using Oleic acid, the first injected slurry would easily cross the needle but at a certain point a solid residue would accumulate in the syringe and only solvent would be extruded (phase separation). PVA at 5% was discontinued as slurries containing it were incapable of being extruded by the 0,7 mm needle.

When Sodium alginate was incorporated in the phosphate buffer solution at 2,5%, the slurries exhibited an interesting characteristic that was only noticed later. Slurries containing alginate and Tween 20, if well isolated in a syringe, wouldn't become stiffer or harder to extrude as time passed. One of the syringes was sealed and kept at room temperature for 3 weeks and then tested, and the extrusion through a 0,7 mm needle was still possible.

By the observation of the Figure 4.6 (F) it is possible to notice that when the following filament/layer comes in contact with the previous ones, their structure was not affected and still adhered to each other.

Table 4.4 presentes some results for the final optimization with the final components.

Table 4.4 – Useful printing time study on the slurries combinations. (* - Phosphate buffer solution with a 2,5% Alginic acid w/w)

Bioglass powder (g)	Glycerine (mL)	Tween 20 (mL)	Phosphate buffer solution (mL)	Useful printing time (min)
0,5	-	-	0,75	10
0,5	-	0,2	0,6	17
0,5	0,1	0,2	0,6	12
0,5	0,2	0,2	0,6	15
0,5	-	0,3	0,6	20
0,5	-	0,2	0,7 *	>100
0,5	-	-	0,8 *	8
0,5	-	-	1 *	11
0,5	-	0,25	0,6 *	>100
0,5	-	0,25	0,75 *	>100

The several components were chosen due to the good feedback reported in some ongoing works. After many different ratio combinations of these components, Tween 20 provided the best printing results. The addition of alginic acid to the buffer solution allowed for a much smother paste with an indefinite extrusion time (> 3 weeks), as the paste wouldn't solidify if well isolated

inside the syringe to prevent contact with the air. The final composition with quantities used to fill one syringe was: 1,5 g of bioglass powder + 0,75 mL of Tween 20 + 2,25 mL Buffer solution > ~ 3,4 mL of slurry.

In the production of this slurry, first the bioglass powder and the Tween 20 were well mixed with a spatula in a glass flask for 3 to 5 minutes until no liquid remained visible. Then, the Buffer solution was added and after 3 minutes of mixing with a spatula the white homogeneous slurry was ready to be printed.

4.5.1.2 Printing parameters

Several adjustments had to be made respecting to this procedure. In Appendix IV all of the parameters used in the final structure's prints are shown. As the printer is not prepared to sustain smaller nozzle diameters besides the incorporated in the extruder, discrepancies in the relations between layer height and filament diameter, for example, can be encountered.

4.5.2 Optical microscopy and Scanning Electron Microscopy (SEM)

After the printing and sintering processes, various samples were observed to check if structure and porosity weren't compromised by the evaporation of the slurry solvents. As Figure 4.7 reveals, rugosity of the samples' surface is high and some structural flaws were visible due to the evaporation of solvents and to the defective infill of the printing pattern.



Figure 4.7 – Optical microscope image of the wall of a sintered 3D printed structure.

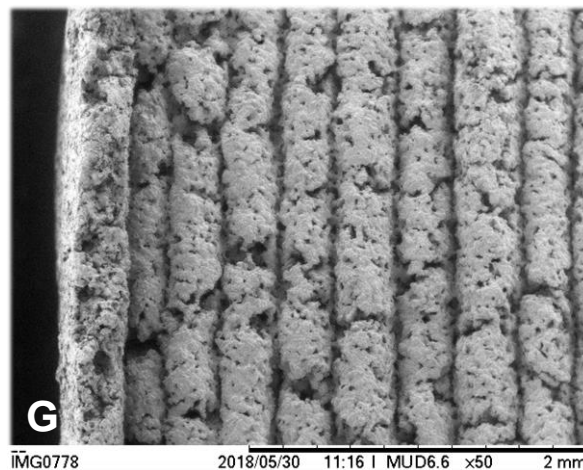


Figure 4.8 – SEM image of the side view (G) of sintered structures.

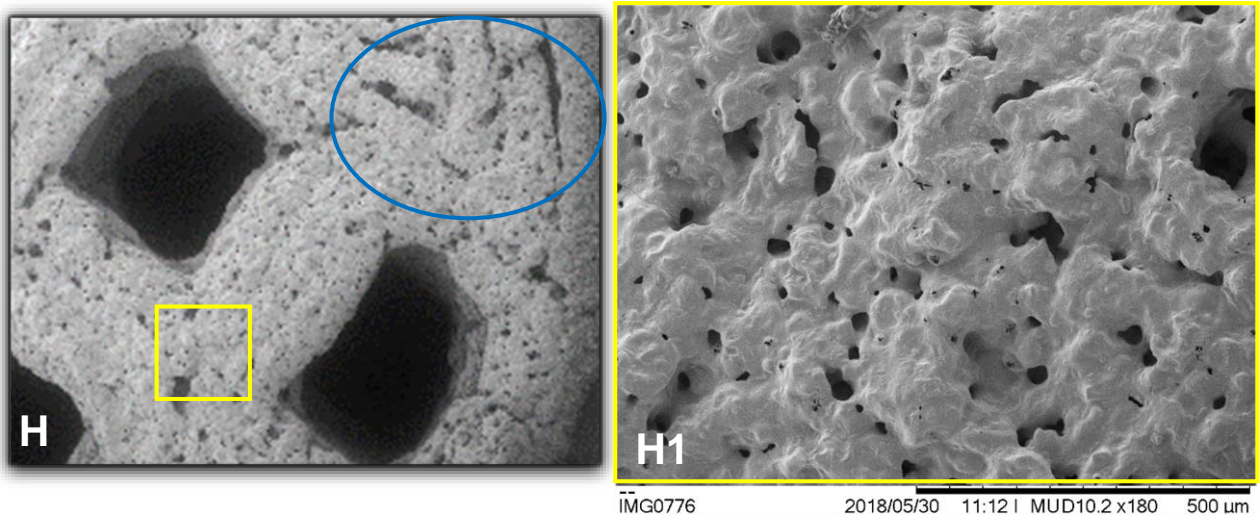


Figure 4.9 – SEM images of the top surface of structures sintered at 1100 °C.

Through the observation of the SEM images it was possible to notice that each layer was connected to the adjacent ones (G). SEM images also revealed that the contact area of each layer was not yet maximized as flaws could be observed. Different pore sizes were present but some of the larger ones (H, blue) were related to printing flaws that still needed to be improved by changing printing speed, extrusion speed or infill percentage. In a more detailed observation (H1) the micro porosity could be evaluated and measurements gave pore sizes between 5 and 100µm.

4.5.3 DSC-TG

Differential scanning calorimetry as well as a thermogravimetric study were made on the mesoporous 80S5P15C bioglass powder and on the final cement composition to evaluate their behaviour under sintering conditions. The bioglass powder used in these studies had already been thermally treated at 600 °C to burn all the Pluronic F-127.

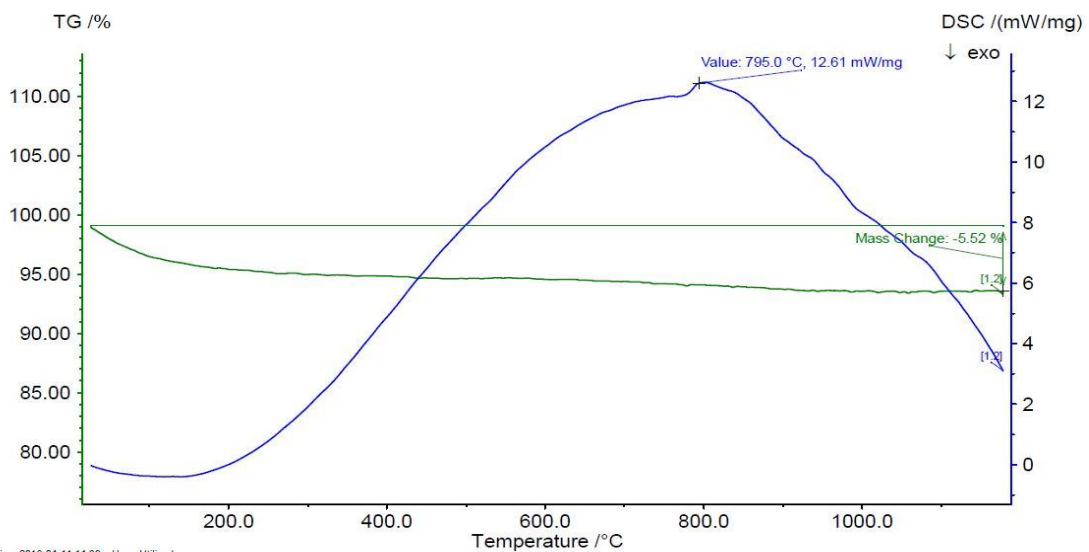


Figure 4.10 – DSC-TG graphic analysis of the mesoporous 80S5P15C bioglass powder after 600 °C treatment for 2 hours.

In Figure 4.10 it was possible to observe that mass loss was not very significant, since the major loss occurred until 200 °C, indicating that absorbed water was probably present. No obvious glass transition or densification could be inferred from DSC-TG results.

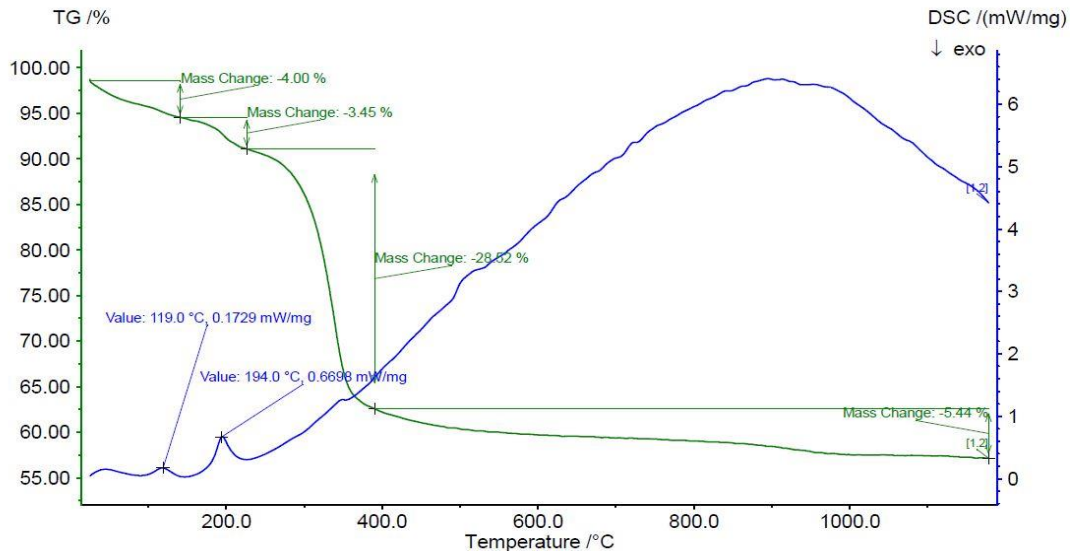


Figure 4.11 – DSC-TG graphic analysis of the mesoporous 80S5P15C bioglass cement after 24h drying process at 60 °C.

In Figure 4.11, the first 2 peaks represent mass losses at 119 °C and 194 °C corresponding to water and Tween 20 evaporation, respectively. The third and larger mass loss, could possibly represent the melting of Sodium Alginate used in the buffer solution. [27]

4.5.4 X-Ray Diffraction

With the help of the Match! Software crystalline phases were identified in the cement diffractogram.

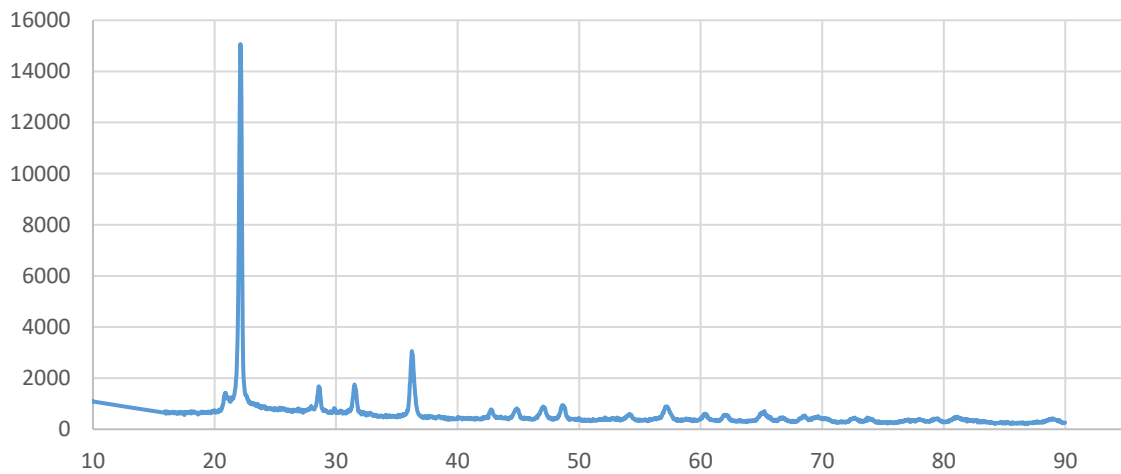


Figure 4.12 – Diffractogram of the final cement composition after thermal treatment at 1100 °C.

Limiting the search parameters in the software to phases that only contain the elements H, C, N, O, Na, Si, P, Cl and Ca, cristobalite (SiO₂) was the most probable match found with a 93%

match. Any other possible phases indicated by the matching software were not taken into account since it is recommended to only consider phases with more than 80% match.

4.5.5 FTIR

Two FTIR analysis were made on the mesoporous 80S5P15C bioglass after the thermal treatment at 600 °C, and to the cement after 1100 °C.

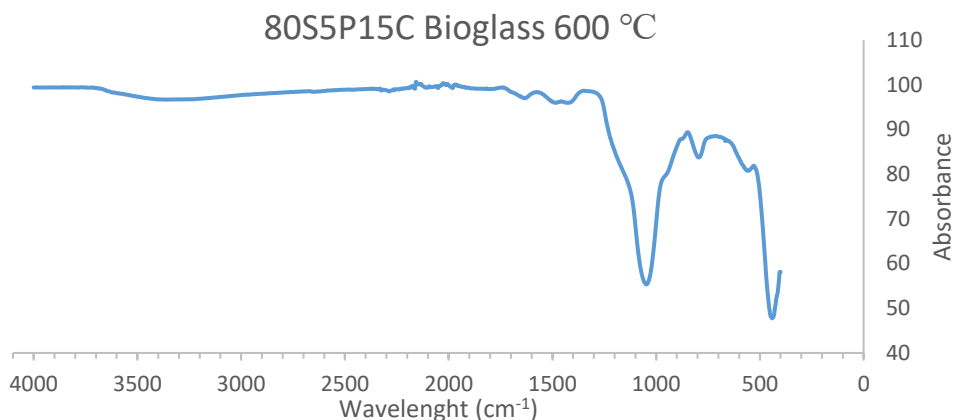


Figure 4.13 – FTIR spectrum of the mesoporous 80S5P15C bioglass (600 °C).

In the spectrum represented in Figure 4.13, a small band at 600 cm^{-1} is related to amorphous P-O, and its presence could indicate the existence of amorphous calcium phosphates [28]. Silicate absorption bands were present near to 500, 800 and 1080 cm^{-1} [29]. Hidden by the Si-O-Si bands, smaller PO_4 bands were probably present [30]. Between 3700 and 2750 cm^{-1} a large band was observed and probably corresponds to water adsorption as explained by I. Notingher et al. [28]. Mesoporosity of the bioglass particles can be responsible for water absorption.

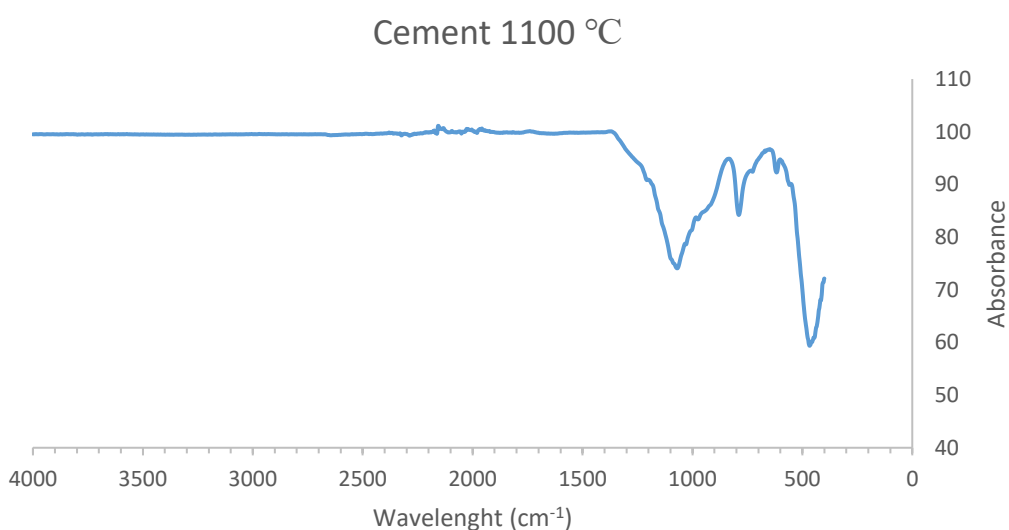


Figure 4.14 – FTIR spectrum of the bioglass cement treated at 1100 °C.

In the FTIR spectrum of the final material sintered at 1100 °C, the main noticeable change was the absence of the adsorbed water band detected in the bioglass FTIR. As it was observed, peaks relative to Figure 4.13 are still present in the cement FTIR spectrum.

4.5.6 Mechanical characterization

4.5.6.1 Compressive strength and elastic modulus

For mechanical properties evaluation, only 5 samples were tested due to some unexpected problems regarding the shape of the samples after thermal treatment. Even though the number was not very significant to make a statistical analysis, the results were very consistent without considerable variation between the maximum force registered before fracture (1,56 to 1,75 kN).

The average maximum force sustained before fracture was 1,7 kN, which corresponded to a stress of 6,5 MPa. As compressive strength of trabecular bone lies in the 2 to 12 MPa interval, the value for the tested material is considered good as it offers a similar behaviour. Figure 4.15 shows the typical compression curve obtained for the printed structures. In this curve, three regions can be observed: elastic, collapse and densification.

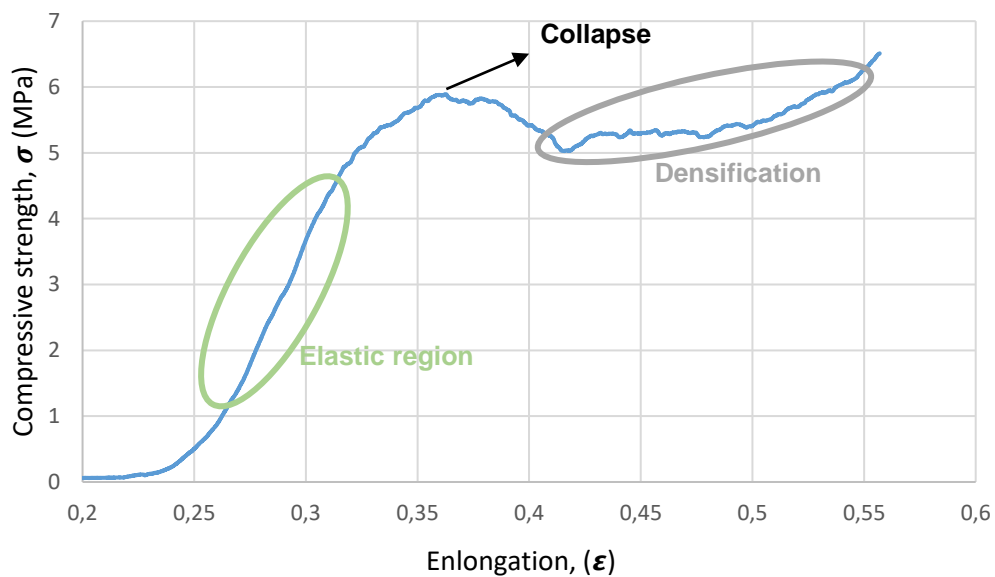


Figure 4.15 – Compression curve of a bioglass cement sample after 1100 °C sintering process.

From the slope of the elastic region, the Young modulus was obtained with a value of $79,7 \pm 14,8$ MPa, which is within the trabecular bone values (50 to 500 MPa), but very near the inferior limit [31].

4.5.6.2 Porosity study (Archimedes method)

Several measurements were made to evaluate the behaviour of the cement material after thermal treatment. Using the Archimedes method to calculate the density and porosity of cylindrical pellets and printed structures, the following table resumes the obtained results.

Table 4.5 – Study on the densification and porosity of the material.

	m_{dry} (mg)	$m_{immerse}$ (mg)	m_{humid} (mg)	Open volume (mm ³)	Total volume (mm ³)	Density (g/cm ³)	Microporosity
900 °C	293	146	341	48	195	1,5	24,6%
1000 °C	300	141	343	43	198	1,52	21,7%
1100 °C	313	169	362	49	193	1,62	25,4%
Structure 1100 °C	867	441	1048	181	607	1,43	29,8%

Even though a relation between the apparent porosity results with the sintering temperature couldn't be established, the relative density showed a slight increment with the increase of temperature. It is important to state that this open porosity measuring method lacked some accuracy due to the difficulty to saturate the pore network with the fluid, in this case distilled water. In another point of view, the porosity measured in the printed structure only took into account the pores in the solid parts (walls) of the sample, despising the hollow areas (voids in Figure 4.16). Besides the fact that these voids result in an increase in the superficial area, an estimation of the real porosity was made.

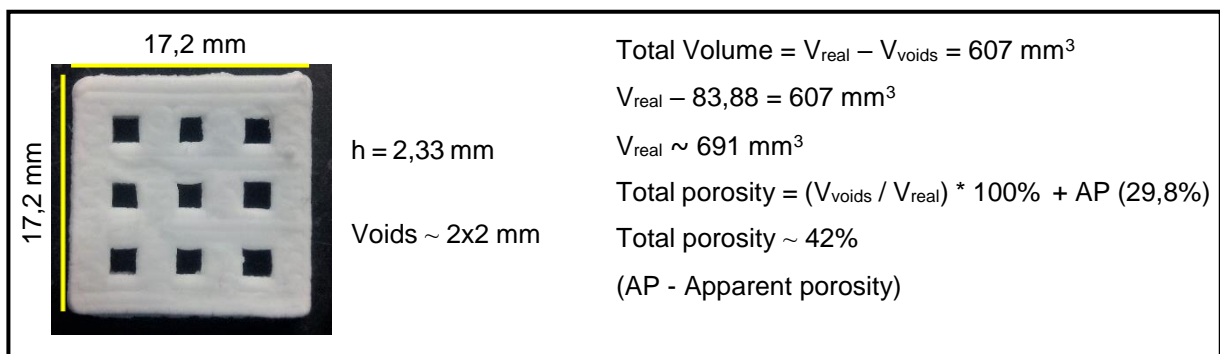


Figure 4.16 – Top view of an example structure used in the porosity evaluation with measures and calculations of the real volume.

Upon analysis, and knowing the compressive strength of the produced structures, a comparison was made with a review article by Fu, Qiang et al. [18]. In the following figure a collection of studies on the compressive strength and porosity of several bioactive glass scaffolds are presented.

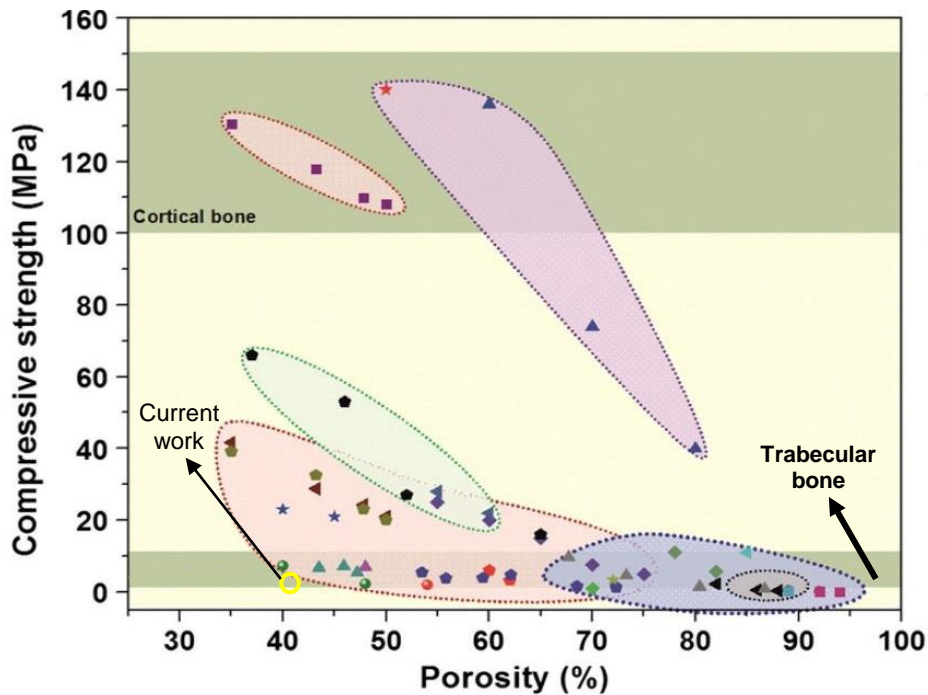


Figure 4.17 – Studies on the porosity and compressive strength of bioactive glass scaffolds. Adapted from [18].

The produced structures in the current work are marked in yellow. As it was possible to observe, the characteristics of the resulting material are consistent with the values for trabecular bone but significantly far from the porosity of 3D structures produced in other works. The comparison between the structures made in this work with the structures represented in the Figure 4.17 is not easy, as none of them are relative to a rapid prototyping production method like 3D printing of bioglass cement. Yet, comparing with the two of the closest studies within the trabecular bone area (▲ for Shih-Ching Wu et al. [32] and ● for Qiang Fu et al. [33]) a 7~8% porosity difference is noticeable. Both of these articles used melt-derived bioglasses, 45S5 and 13-93 bioglasses respectively, which normally provides better mechanical properties to the final scaffolds, and use a form of replication technique and a particle leaching technique to produce the scaffolds. These techniques easily allow for a much better porosity control as the inserted sacrificial particles will leave voids in the material, and in the replication case the porosity depends on the sacrificial template. In the current work pores are a result of solvents evaporation plus the structural printed voids which count as free space also.

4.5.7 Cytotoxicity

The first cytotoxicity tests encountered some setbacks relative to samples degradation in the culture medium. Beforehand, the samples degradation behaviour was only tested in water and the final result gave a positive feedback, as no physical alterations were visible after 2 weeks. After obtaining the knowledge that culture medium would disaggregate the samples, a second degradation test was made with salty water, which after a few hours revealed some physical damage to the structure and small particle disassociation. If shaken, the solution would become

a suspension of the disassociated particles, even though the structure was maintained. However, after a few minutes particles would sediment. Although this fact could compromise the final results, a second cytotoxicity test was performed with care to not extract any particles.

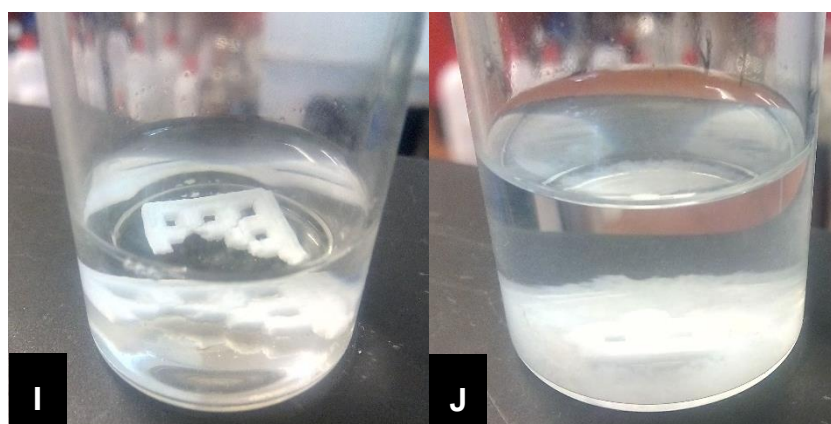


Figure 4.18 – Degradation tests in Water (I) and a NaCl solution (J) after 2 weeks.

In the second test, another problem was detected. The material revealed to be very acid when tested with an indicator (Phenol red). The extract turned yellow indicating that the pH was much lower than 7, with an estimated value between 1 and 2 . A neutralization process of the extract was performed by the addition of Sodium Hydroxide (NaOH), but without any success, since after neutralization the extract turned acid again. The acidity could be linked to the use of HCl in the production of the mesoporous bioglass and the use of Alginic acid in the cement slurry. An attempt to overcome this problem consists in the dialysis treatment of the powder after the thermal step at 600 °C. Another alternative would be the use of a lower molarity acid in the bioglass synthesis. This would imply a longer reaction time for the bioglass sol-gel to form as the acid is a catalyst of the reaction.



Figure 4.19 – Extract with pH indicator (Phenol red) after neutralization attempt. Yellow colour indicating an acid solution.

5 Conclusion and Future perspectives

In this work three distinct production methods to produce bioglass porous structures were studied.

After several attempts to produce ICCs through impregnation of bioglass sol-gel into Polystyrene CCs, none was capable of producing such a structure. Besides the lack of connection between bioglass particles after the sintering processes, Bioglass sol-gel with sodium in its composition revealed to be very brittle, even when sintered in the form of cylindrical tablets, made by applying 2 tons of compressive force. Bioglass production without sodium content revealed to be much stiffer compared to the regular 45S5 Bioglass and the half sodium content bioglass. Densification of the 45S5 Bioglass was assessed and its peak value was found between 1000 and 1050 °C. Above 1050 °C melting of the material was noticeable.

In the freeze-drying production method some structures were produced with partial success. As there was no unidirectional freezing equipment, the porous structures became disorganized and with pores of different sizes. Therefore, these structures didn't offer enough mechanical resistance and had to be handled with extra caution. A sintering process was made to make an attempt to densify the material but without success.

The 3D printing technique allowed for more robust structures to be produced. After the optimization of the slurry's composition and after some corrections to the extruding parameters, different designs were printed to evaluate the precision of the printer. It was possible to print pieces with an accuracy of 0,5 mm (the nozzle diameter) but the success ratio was too low and required further optimization, given this, the nozzle diameter used to print the characterized pieces was 0,7 mm.

Through optical microscopy it was observed that the pieces surface was very rough due to the mesoporosity of the bioglass particles and the evaporation of both Tween 20 and alginate during sintering. The SEM images showed that pores with sizes between 10 and 100 μm were achieved with this method.

Mechanical characterization revealed that the final designed pieces presented an average compression strength of 6,5 MPa. This could be considered a good result, given that trabecular bone's compressive strength fluctuates between 2 and 12 MPa. Yet, as only 5 samples were tested, this result requires further evaluation. Young's modulus was also calculated and a value around 80 MPa was obtained, which is near the lower limit of the interval for trabecular bone (50 to 500 MPa), but nonetheless, within the range. Through an improvement in the printing parameters it would still be possible to increase these values, given that printing flaws such as air bubbles inside the syringe, little bumps that were visible in the impression plate, some heterogeneity of the slurry and different bioglass particles size (which studies weren't made) were still present.

Cytotoxicity tests were attempted with the extract and resazurin method in two equal samples. These two tests revealed two different problems: a) the degradation rate of the material in culture medium and b) the acidity of the same material. The acidity of the material could be explained by the use of HCl in the bioglass production, which then affects the pH of the culture medium. To overcome this problem a neutralization was attempted but after some time the extract turned acid once again. The degradation rate problem could also be an implication of the high acidity of the material. When in contact with higher pH solutions salts are probably produced to stabilize and neutralize the solution.

There is still a lot of room to improve and optimize these processes with emphasis in the 3D printing method. In the current work the equipment used was not ideal and several adjustments had to be made. This implies that a change in any of the resources used could result in another optimization process completely different from the applied in this work.

As future perspectives, several additional studies could be made for a better understanding of the bioglass cement mix:

- Slurry optimization for more detailed printing with smaller nozzle diameter. This optimization could lead to the possibility of producing more precise pores and to better control the open porosity of the material without only relying on the solvents evaporation;
- Evaluate the variation of the porosity of the structures with the solid : liquid ratio of the slurry;
- DRX studies of samples immersed in SBF during different periods of time to evaluate the formation of crystalline phases indicative of bioactivity;
- Evaluate particle size and study its relation with compressive strength of printed structures;
- Degradation tests in SBF during different periods of time to evaluate the durability of the material and to predict its behaviour *in vivo*;
- Study of the optimal thermal treatment conditions to combine the better mechanical resistance with the better biological results. Further investigation for temperatures above 1100 °C;
- To surpass the acidity problem, lower the molarity or use a weak acid to produce the bioglass powder. A deacidification process after bioglass powder production can also be done (eg: dialysis).

6 Bibliography

- [1] L. L. Hench, R. J. Splinter, W. C. Allen, and T. K. Greenlee, "Bonding mechanisms at the interface of ceramic prosthetic materials" *J. Biomed. Mater. Res.*, vol. 5, no. 6, pp. 117–141, 1971.
- [2] J. Faure *et al.*, "A new sol-gel synthesis of 45S5 bioactive glass using an organic acid as catalyst" *Mater. Sci. Eng. C*, vol. 47, pp. 407–412, 2015.
- [3] L. L. Hench, "The story of Bioglass®" *J. Mater. Sci. Mater. Med.*, vol. 17, no. 11, pp. 967–978, 2006.
- [4] C. F. C. João, J. M. Vasconcelos, J. C. Silva, and J. P. Borges, "An Overview of Inverted Colloidal Crystal Systems for Tissue Engineering" *Tissue Eng. Part B Rev.*, vol. 20, no. 5, pp. 437–454, 2014.
- [5] J. R. Jones, "Reprint of: Review of bioactive glass: From Hench to hybrids" *Acta Biomater.*, vol. 23, no. S, pp. S53–S82, 2015.
- [6] M. N. Rahaman *et al.*, "Bioactive glass in tissue engineering" *Acta Biomater.*, vol. 7, no. 6, pp. 2355–2373, 2011.
- [7] H. Shirahama *et al.*, "Fabrication of Inverted Colloidal Crystal Poly(ethylene glycol) Scaffold: A Three-dimensional Cell Culture Platform for Liver Tissue Engineering" *J Vis Exp*, no. 114, pp. 1–12, 2016.
- [8] D. Hutmacher, T. Woodfield, P. Dalton, and J. Lewis, "Chapter 14 - Scaffold design and fabrication A2 - Blitterswijk, Clemens van" pp. 403–454, 2008.
- [9] J. H. Gilmore, "NIH Public Access" *North*, vol. 29, no. 10, pp. 1883–1889, 2008.
- [10] M. C. Gutiérrez, M. L. Ferrer, and F. Del Monte, "Ice-templated materials: Sophisticated structures exhibiting enhanced functionalities obtained after unidirectional freezing and ice-segregation-induced self-assembly" *Chem. Mater.*, vol. 20, no. 3, pp. 634–648, 2008.
- [11] X. Zhang, C. Li, and Y. Luo, "Aligned/unaligned conducting polymer cryogels with three-dimensional macroporous architectures from ice-segregation-induced self-assembly of PEDOT-PSS" *Langmuir*, vol. 27, no. 5, pp. 1915–1923, 2011.
- [12] J. Li, L. Nie, Z. Li, L. Lin, L. Tang, and J. Ouyang, "Maximizing modern distribution of complex anatomical spatial information: 3D reconstruction and rapid prototype production of anatomical corrosion casts of human specimens" *Anat. Sci. Educ.*, vol. 5, no. 6, pp. 330–339, 2012.
- [13] Y. AbouHashem, M. Dayal, S. Savanah, and G. Štrkalj, "The application of 3D printing in anatomy education" *Med. Educ. Online*, vol. 20, no. 1, pp. 1–4, 2015.
- [14] V. Baskaran, G. Štrkalj, M. Štrkalj, and A. Di Ieva, "Current Applications and Future Perspectives of the Use of 3D Printing in Anatomical Training and Neurosurgery" *Front.*

- Neuroanat.*, vol. 10, no. June, pp. 1–7, 2016.
- [15] Y. Minaberry and M. Jobbágy, “Macroporous bioglass scaffolds prepared by coupling sol-gel with freeze drying” *Chem. Mater.*, vol. 23, no. 9, pp. 2327–2332, 2011.
- [16] R. Surace, L. A. C. De Filippis, E. Niini, A. D. Ludovico, and J. Orkas, “Morphological investigation of foamed aluminum parts produced by melt gas injection” *Adv. Mater. Sci. Eng.*, vol. 2009, no. March, 2009.
- [17] J. M. Williams *et al.*, “Bone tissue engineering using polycaprolactone scaffolds fabricated via selective laser sintering” *Biomaterials*, vol. 26, no. 23, pp. 4817–4827, 2005.
- [18] Q. Fu, E. Saiz, M. N. Rahaman, and A. P. Tomsia, “Bioactive glass scaffolds for bone tissue engineering : state of the art and future perspectives” vol. 31, pp. 1245–1256, 2011.
- [19] T. Livingston, P. Ducheyne, and J. Garino, “In vivo evaluation of a bioactive scaffold for bone” pp. 1–13, 2001.
- [20] B. Sui, G. Zhong, and J. Sun, “Evolution of a Mesoporous Bioactive Glass Scaffold Implanted in Rat Femur Evaluated by ⁴⁵Ca Labeling, Tracing, and Histological Analysis” 2014.
- [21] X. Liu, M. N. Rahaman, and Q. Fu, “Acta Biomaterialia Bone regeneration in strong porous bioactive glass (13-93) scaffolds with an oriented microstructure implanted in rat calvarial defects” *Acta Biomater.*, vol. 9, no. 1, pp. 4889–4898, 2013.
- [22] T. Zhu *et al.*, “Novel bioactive glass based injectable bone cement with improved osteoinductivity and its in vivo evaluation” *Sci. Rep.*, vol. 7, no. 1, pp. 1–10, 2017.
- [23] S. Midha, T. Bo, W. Van Den Bergh, P. D. Lee, J. R. Jones, and C. A. Mitchell, “Acta Biomaterialia Preconditioned 70S30C bioactive glass foams promote osteogenesis in vivo” *Acta Biomater.*, vol. 9, no. 11, pp. 9169–9182, 2013.
- [24] J. R. Jones, L. M. Ehrenfried, and L. L. Hench, “Optimising bioactive glass scaffolds for bone tissue engineering” vol. 27, pp. 964–973, 2006.
- [25] S. W. Choi, I. W. Cheong, J. H. Kim, and Y. Xia, “Preparation of uniform microspheres using a simple fluidic device and their crystallization into close-packed lattices” *Small*, vol. 5, no. 4, pp. 454–459, 2009.
- [26] Y. Luo, C. Wu, A. Lode, and M. Gelinsky, “Hierarchical mesoporous bioactive glass/alginate composite scaffolds fabricated by three-dimensional plotting for bone tissue engineering” *Biofabrication*, vol. 5, no. 1, 2013.
- [27] J. P. Soares, J. E. Santos, G. O. Chierice, and E. T. G. Cavaleiro, “Thermal behavior of alginic acid and its sodium salt” *Ecl Quim*, vol. 29, no. 2, p. 53, 2004.
- [28] I. Notingher *et al.*, “Application of FTIR and Raman Spectroscopy to Characterisation of Bioactive Materials and Living Cells” *Spectrosc. Int. J.*, vol. 17, no. 2–3, pp. 275–288, 2003.

- [29] G. M. Luz and J. F. Mano, "Preparation and characterization of bioactive glass nanoparticles prepared by sol-gel for biomedical applications" *Nanotechnology*, vol. 22, no. 49, 2011.
- [30] Y. Rezaei, F. Moztarzadeh, S. Shahabi, and M. Tahiri, "Synthesis, Characterization, and *In Vitro* Bioactivity of Sol-Gel-Derived SiO_2 - CaO - P_2O_5 - MgO - SrO Bioactive Glass" *Synth. React. Inorganic, Met. Nano-Metal Chem.*, vol. 44, no. 5, pp. 692–701, 2014.
- [31] J. Henkel *et al.*, "Bone Regeneration Based on Tissue Engineering Conceptions — A 21st Century Perspective" *Bone Res.*, vol. 1, no. 3, pp. 216–248, 2013.
- [32] S. C. Wu, H. C. Hsu, S. H. Hsiao, and W. F. Ho, "Preparation of porous 45S5 Bioglass®-derived glass-ceramic scaffolds by using rice husk as a porogen additive" *J. Mater. Sci. Mater. Med.*, vol. 20, no. 6, pp. 1229–1236, 2009.
- [33] Q. Fu, M. N. Rahaman, B. Sonny Bal, R. F. Brown, and D. E. Day, "Mechanical and in vitro performance of 13-93 bioactive glass scaffolds prepared by a polymer foam replication technique" *Acta Biomater.*, vol. 4, no. 6, pp. 1854–1864, 2008.
- [34] H. Yan, K. Zhang, C. F. Blanford, L. F. Francis, and A. Stein, "In vitro hydroxycarbonate apatite mineralization of CaO - SiO_2 sol-gel glasses with a three-dimensionally ordered macroporous structures" *Chem. Commun.*, vol. 13, no. 22, pp. 1374–1382, 2001.
- [35] Q. Shi, J. Wang, J. Zhang, J. Fan, and G. D. Stucky, "Rapid-setting, mesoporous, bioactive glass cements that induce accelerated in vitro apatite formation" *Adv. Mater.*, vol. 18, no. 8, pp. 1038–1042, 2006.

Appendix I

Bioglass production

45S5 Bioglass

26 mL of nitric acid (1M) were put into a beaker under stirring at 40 °C. 11,6 mL of Tetraethyl orthosilicate (TEOS) and 1 mL of Triethyl Phosphate (TEP) were mixed and added drop by drop into the beaker. 4,66 g of Sodium Nitrate (NaNO_3) and 7,15 g of Calcium Nitrate tetrahydrate ($\text{Ca}(\text{NO}_3)_2 \cdot 4\text{H}_2\text{O}$) were also slowly added in the respective order, until a clear sol was obtained [2]. After the gelling process, for CCs impregnation the gel was left sealed at room temperature, and for powder production the sol-gel was left in an oven at 60 °C for 12h. Afterwards the powder was heated at 200 °C for 5h, and finally at 700 °C for 2h.

80S20C Bioglass

Using the same reagents as 45S5 Bioglass and under vigorous stirring, 4,72 g of ($\text{Ca}(\text{NO}_3)_2 \cdot 4\text{H}_2\text{O}$) was dissolved in 12 mL nitric acid at room temperature. Then, 16,67 g of TEOS was added to obtain a 80 mol % SiO_2 and 20 mol % CaO. The solution was left under stirring until a sol-gel was formed [34].

80S5P15C (Si:P:Ca) Bioglass

Mesoporous 80S5P15C (Si:P:Ca) Bioglass

Under light magnetic stirring (~60 rpm), an acidic solution was prepared with 48,4 mL of ethanol, 14,4 mL of Millipore water and 4,8 mL of hydrochloric acid (1M). After homogenization 32,3 mL of TEOS and 1,5 mL of TEP were added drop wise in this order. Finally, 6,49 g of Calcium nitrate were dissolved in the solution. Once the solution was completely clear, 11,43 g of Pluronic F-127 were slowly added under vigorous stirring until total dissolution. Stirring was stopped and the sol-gel was left to dry in an oven for 48 hours at 60 °C. Sintering of the resulting glass particles was made at 600 °C for 2h. A 30 minute milling step in an agate mortar (Mini Mill II) followed the thermal treatment to diminish particle size. This procedure was based on the production method mentioned in Shi *et al* [35].

Regular 80S5P15C (Si:P:Ca) Bioglass

10,26 mL of TEOS and 0,56 g of TEP were added to 3,48 mL of HNO_3 (0,06M) and left stirring for 1 day. After that, the same volume of water was added and the solution was left under low pressure at 40 °C for ethanol removal. The ethanol removal process duration was not consistent due to the different sizes of the beakers. In the next step portions of the initial solution (1,41 mL) were taken into smaller flasks and 0,33 mL of a saturated Calcium nitrate solution was added. Finally, different amounts of water were also added to make 10, 12,5 and 15% solid content sol-gel solutions.

Reagents:

- Tetraethyl orthosilicate ($\text{Si}(\text{OC}_2\text{H}_5)_4$), Aldrich;
- Triethyl Phosphate ($(\text{PO}(\text{C}_2\text{H}_5)_3)$, Fluka Analytical;
- Sodium Nitrate (NaNO_3), Panreac;
- Calcium Nitrate tetrahydrate ($\text{Ca}(\text{NO}_3)_2 \cdot 4\text{H}_2\text{O}$), VWR Chemicals;
- Nitric Acid (HNO_3), Panreac, 65%;
- Absolute Ethanol ($\text{C}_2\text{H}_6\text{O}$), Honeywell, 99,8%;
- Hydrochloric acid (HCl), Carlo Erba, 37%;
- Pluronic F-127, Sigma.

Appendix II

Microspheres production

Polystyrene (PS) microspheres were produced using a microfluidic system made by a continuous and a discontinuous phase, Poly(vinyl alcohol) (PVA) 5% in water and PS 5% in dichloromethane respectively. After several hours of production, spheres were dried and cleaned in 2-propanol. Following a stage of sieving to obtain short intervals of diameters, they were observed under the microscope to evaluate their shape. After that, several sets of 40 mg of spheres were arranged in cylindrical containers of 5,93 mm of diameter (Figure 3.1) with drops of ethanol. A 15 minutes of ultra-sounds stage was performed and 1 hour in orbital shaking to obtain a hexagonal close packed structure. In the same recipient they were annealed in an oven for 4 hours at 130 °C.

Reagents:

- Poly(vinyl alcohol) $(C_2H_4O)_x$, Acros Organics, $M_w \sim 95,000$;
- Polystyrene $(C_8H_8)_n$, Aldrich, $M_w \sim 350,000$;
- Dichloromethane CH_2Cl_2 , Sigma-Aldrich, 99.9%.

Appendix III

CCs impregnation

Manual impregnation was performed using a spatula to force the bioglass gel into the vacancies of the CC. A portion of a 25% PVA in acetone solution was mixed with 3 separated bioglass gels to get the 0,25%, the 0,75% and 1,25% of PVA. Normal BG gel and the PVA/BG mixes were used not only on manual impregnation but also in vacuum and centrifuge cycles.

Vacuum impregnation with BG gel was performed in a flask containing the gel and several CCs inside of it. Vacuum was also used during synthesis of the BG gel with CCs inside the solution.

Different centrifuge cycles were performed from only 1 to a maximum of 9, and the mass evolution was studied between every cycle. At every cycle, CCs were carefully removed from the test tubes, excess gel was removed and then CCs were dried in an oven at 60 °C for at least 12h before mass measuring. Each cycle represents 10 minutes at 4000 RPMs, which corresponds to ~2500 g.

Using a spatula, an amount of BG gel was added to a syringe containing a CC near the nozzle, the piston was pressed and the gel forced to go through the CC.

Appendix IV

3D printing parameters

Quality			
Layer Height	↻	0.5	mm
Initial Layer Height	↻	0.5	mm
Line Width	↻ i	0.95	mm
Wall Line Width		0.95	mm
Outer Wall Line Width		0.95	mm
Inner Wall(s) Line Width		0.95	mm
Top/Bottom Line Width		0.95	mm
Infill Line Width		0.95	mm
Skirt/Brim Line Width		0.95	mm
Shell			
Wall Thickness	↻	0.7	mm
Top/Bottom Thickness	↻	0.7	mm
Infill			
Infill Density	↻	100	%
Infill Pattern	↻ i	Lines	▼
Infill Overlap Percentage	↻ i	0	%
Material			
Printing Temperature	↻ i	0	°C
Diameter	↻	0.7	mm
Flow		100	%

Enable Retraction	<input checked="" type="checkbox"/>
Speed	
Print Speed	↻ 7 mm/s
Travel Speed	↻ i 10 mm/s
Travel	
Support	▼
Enable Support	<input type="checkbox"/>
Build Plate Adhesion	
Build Plate Adhesion Type	Skirt ▼
Skirt Line Count	↻ 2
Skirt Distance	3 mm
Skirt/Brim Minimum Length	↻ 3 mm



Figure 20 - Hyrel 30M 3D printer

The software used to define the printing parameters was Cura (version 2.5.0), and the design software was Tinkercad Online, (www.tinkercad.com).

Buffer Solution composition: 60,1 g $(\text{NH}_4)_2\text{HPO}_4$ + 5,0 g $\text{NH}_4\text{H}_2\text{PO}_4$ + 100 mL H_2O + 2,5 g Alginate.

Reagents:

- Pharmaceutical Glycerine;
- Tween 20 ($\text{C}_{58}\text{H}_{114}\text{O}_{26}$), VWR Chemicals, $M_w \sim 1,250$;
- Oleic Acid;
- Alginic Acid Sodium Salt ($\text{C}_6\text{H}_7\text{O}_6\text{Na}$)_n, Panreac;
- Ammonium di-Hydrogen Phosphate ($(\text{NH}_4)_2\text{H}_2\text{PO}_4$), Panreac;
- Ammonium Phosphate dibasic ($(\text{NH}_4)_2\text{HPO}_4$), Sigma-Aldrich.

Appendix V

Cytotoxicity and cell viability

A sample was immersed in culture medium for more than 24h at 37 °C. As the tested material is a ceramic, the ratio (mass of sample)/(volume of culture medium) was set to around 100 mg/ml, as recommended. The extract was then moved to the cell seeding wells and let for incubation for more than 24h following the ISO 10993-5 regulation. The cytotoxic positive control has in its constitution cells in normal culture medium to which has been added Dimethyl sulfoxide at 10%. The non-cytotoxic negative control has only cells in normal culture medium.

For the cell viability test the culture medium is aspirated and resazurin (0,04 mg/mL in Phosphate Buffered Saline (PBS)) was mixed with the culture medium in a 1:1 ratio. Resazurin is a non-fluorescent blue colorant which can be used as pH indicator and as cell viability indicator. It is only reduced when a metabolically active cell is present and turns into resorufin which presents a pink colour and high fluorescence. Resazurin, compared to other methods, has the advantage of having a very low level of cytotoxicity. The results were then obtained by measuring the absorbance of the resazurin and resorufin present in the medium. PBS solution used in this test is the same as ThermoFisher 14190 - DPBS, no calcium, no magnesium. (<http://www.thermofisher.com/pt/en/home/technicalresources/mediaformulation.147.html>)

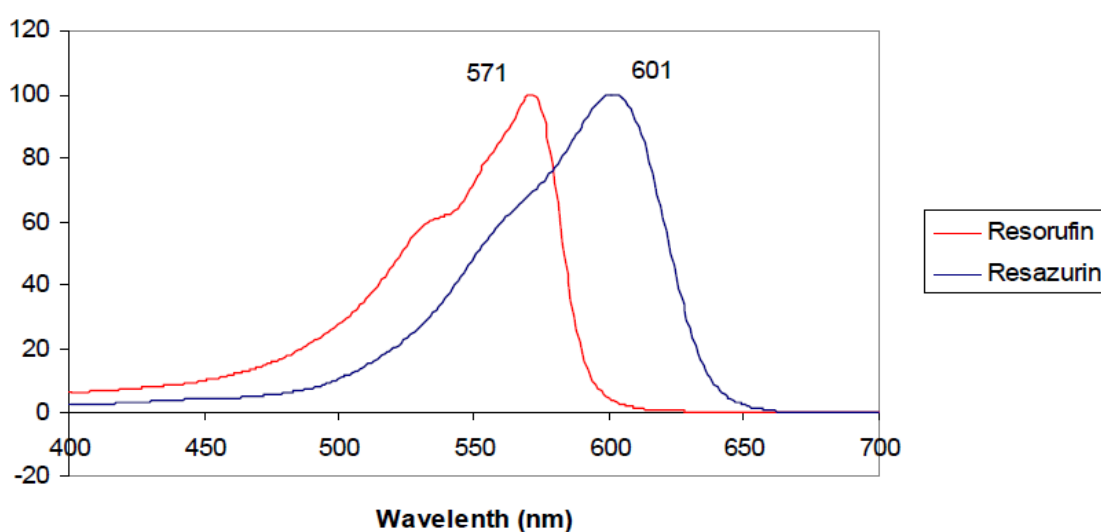


Figure 21 – Absorbance spectrums of resazurin and resorufin.
(<https://tools.thermofisher.com/content/sfs/manuals/PrestoBlueFAQ.pdf>)

The resazurin/resorufin conversion is proportional to the number of metabolic active cells, which is assumed to be the same as the number of viable cells. This number is compared to the number of viable cells of the negative control. The extract toxicity is then expressed according to the relative cell viability:

- Not cytotoxic at $\geq 90\%$
- Slightly cytotoxic from 80% to 89%
- Moderately cytotoxic from 50% to 79%

- Cytotoxic at < 50%